(4)

ARL-AERO-R-173

AR-004-572

DEPARTMENT OF DEFENCE

DEFENCE SCIENCE AND TECHNOLOGY ORGANISATION

AERONAUTICAL RESEARCH LABORATORY

MELBOURNE, VICTORIA

Aerodynamics Report 173

AXISYMMETRIC VORTEX BREAKDOWN PART I CONFINED SWIRLING FLOW (U)

by

J.M. LOPEZ

Approved for Public Release

JANUARY 1988

AR-004-572

DEPARTMENT OF DEFENCE
DEF NCE SCIENCE AND TECHNOLOGY ORGANISATION
AERONAUTICAL RESEARCH LABORATORY

Aerodynamics Report 173

AXISYMMETRIC VORTEX BREAKDOWN PART I: CONFINED SWIRLING FLOW

by

J.M. LOPEZ

SUMMARY

A comparison between the experimental visualization and numerical simulations of the occurrence of vortex breakdown in laminar swirling flows produced by a rotating endwall is presented. The experimental visualizations of Escudier (Experiments in Fluids, 2, 1984) were the first to detect the presence of multiple recirculation zones and the numerical model presented here, consisting of a numerical solution of the unsteady axisymmetric Navier-Stokes equations, faithfully reproduces these newly observed phenomena and all other observed characteristics of the flow. Part II of the paper examines the underlying physics of these vortex flows.

POSTAL ADDRESS: Director, Aeronautical Research Laboratory,
P.O. Box 4331, Melbourne, Victoria, 3001, Australia

CONTENTS

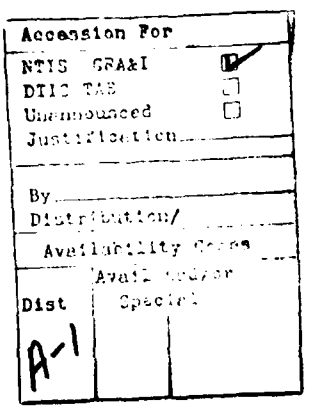

1. Introduction

Vortex breakdown in swirling flows has been the subject of much attention since it was first recognized in the tip vortices of delta winged aircraft (Peckham & Atkinson 1957). More recently it has emerged as a serious problem at high angle of attack for highly manoeuvrable military aircraft. As yet, there is no general consensus on the physical mechanisms responsible for its occurrence. The term vortex breakdown is associated with an abrupt change in the character of a columnar vortex at some axial station. It is usually observed as a sudden widening of the vortex core together with a deceleration of the axial flow and is often followed by a region or regions of recirculation.

Experimental studies of vortex breakdown over delta winged aircraft have been severely hampered by the sensitivity of the flow to the presence of external probes, making quantitative measurements of the flow in the 'burst' regions much more difficult. Further complications arise as a result of the large number of parameters involved, some of which are difficult to measure and/or control and whose importance to the mechanisms leading to vortex breakdown is not known. With the identification of the vortex breakdown of swirling flows in cylindrical tubes (Harvey 1960), a large number of experimental investigations were undertaken (eg. Sarpkaya 1971; Faler & Leibovich 1978; Escudier & Zehnder 1982). A number of distinctive forms of breakdown were observed in these investigations, which also showed the phenomenon typically to be unsteady and possessing various degrees of turbulence and asymmetry. From these results, it had been assumed that a description of vortex breakdown would require a three-dimensional, time dependent calculation of the Navier-Stokes equations albeit with the possibility at high Reynolds numbers of modelling the small scale turbulence.

Recently, Escudier (1984) observed the phenomenon of vortex breakdown in swirling flows in a cylindrical container with a rotating endwall, using a laser-induced fluorescence technique. The experimental results extended those obtained earlier by Vogel (1968) and Ronnenberg (1977) and are the first to be reported in which multiple breakdown bubbles exist in the closed cylindrical geometry. The recirculation bubbles were observed to be axisymmetric and steady over large range of the governing parameters, which re-inforced Escudier's (1984) view, earlier expressed as a result of a series of swirling pipe flow experiments (Escudier & Keller 1983), that vortex breakdown in general is inherently axisymmetric and that departures from axial symmetry result from instabilities not directly associated with the breakdown process. Escudier's experiments

provide a particularly well-defined set of flows in which vortex breakdown occurs and his figures (1984) motivated the present study in which the Navier-Stokes equations are solved numerically under the assumption of axial symmetry. A principal aim of this study was to clarify whether, under the assumption of axial symmetry, the numerical solutions accurately reproduce all of the observed flow characteristics reported by Escudier (1984). A further motivation for undertaking the investigation was to develop a more detailed understanding of the physics of the flow and to clarify features that were not readily resolved from the visualizations. For example, the dye streaks are 'blurred' in the region of critical points in the experiment and the nature of the downstream end of the recirculation bubble is difficult to ascertain from flow visualization. A main reason for this 'blurred' picture is dye diffusion but, in some cases Escudier (1984) noted that certain recirculation zones never develop a well defined internal structure. The numerical study shows that these regions in fact possess a localized low frequency unsteadiness and this unsteadiness would result in a 'blurred' flow visualization.

In part II of this study the physics of the flows is examined in more detail. The solutions are considered from the point of view of standing centrifugal waves and an understanding of the mechanism responsible for the vortex breakdown of these confined swirling flows is presented. The mechanics of vortex breakdown in this particular geometry suggests a generalization which is discussed for some other geometries.

Previous numerical studies of swirling flows confined within a cylindrical container (eg. Pao 1970; Lugt & Haussling 1973; Dijkstra & Heijst 1983) have either been restricted to small aspect ratio flows (H/R, ratio of height and radius of the cylinder, less than 1), or flows with Re, the rotational Reynolds number, too small for vortex breakdown to occur. Lugt & Haussling (1982) is a notable exception in which $H/R < 1.6$, and the occurrence of a single breakdown bubble is reported. Their computational mesh does not appear to be fine enough, however, since they found the size and location of the bubble to vary as the resolution was altered and the time scales of their solutions are not consistent with experimental observations.

Since submitting the first version of this paper, Lugt and Abboud (1987) have also published numerical computations of the vortex breakdown phenomenon produced in an enclosed cylinder by a rotating endwall. Their calculations and those presented here overlap somewhat as both studies use the available experimental results of Escudier (1984) as comparisons for the numerical calculations. The results presented by Lugt and

Abboud (1987) generally agree very well with those presented here and their numerical method of integrating the governing equations is quite different to the present method. A large number of their results had not been integrated forward until a true steady state had been reached and no information regarding the distribution of the azimuthal component of vorticity is presented, which will be shown in Part II of this study to be crucial in understanding the physical mechanism responsible for the vortex breakdown of the vortical core flow.

2. Governing Equations and Boundary Conditions

The flows of interest are simulated by considering a cylinder of radius R and length H, the bottom endwall of which is impulsively started to rotate at constant angular velocity Ω. The fluid, which completely fills the cylinder, is incompressible, of uniform density and a constant kinematic viscosity ν. The axisymmetric form of the Navier-Stokes equations, in cylindrical co-ordinates (r, ϕ, z) with corresponding velocity components (u, v, w), is employed. Time and length are scaled by Ω and $1/R$ respectively.

The system of equations is solved by employing the streamfunction-vorticity formulation, where the pressure does not appear explicitly. This is achieved by the introduction of a streamfunction ψ, where

$$u = -\frac{1}{r}\frac{\partial \psi}{\partial z} \quad \text{and} \quad w = \frac{1}{r}\frac{\partial \psi}{\partial r}, \tag{1}$$

which satisfies continuity and gives for the azimuthal component of vorticity

$$\eta = -\frac{1}{r}\frac{\partial^2 \psi}{\partial z^2} - \frac{\partial}{\partial r}\left(\frac{1}{r}\frac{\partial \psi}{\partial r}\right). \tag{2}$$

Incorporating (1) and (2) in the Navier-Stokes equations leads to the following prediction equations for the azimuthal components of velocity and vorticity together with the prognostic equation for the streamfunction:

$$\frac{\partial v}{\partial t} = \frac{1}{r}J(v) + \frac{1}{r}\frac{v}{r}\frac{\partial \psi}{\partial z} + \frac{1}{Re}\left[\frac{\partial^2 v}{\partial z^2} + \frac{\partial^2 v}{\partial r^2} + \frac{1}{r}\frac{\partial v}{\partial r} - \frac{v}{r^2}\right], \tag{3}$$

$$\frac{\partial \eta}{\partial t} = J\left(\frac{\eta}{r}\right) + 2\frac{v}{r}\frac{\partial v}{\partial z} + \frac{1}{Re}\left[\frac{\partial^2 \eta}{\partial z^2} + \frac{\partial^2 \eta}{\partial r^2} + \frac{1}{r}\frac{\partial \eta}{\partial r} - \frac{\eta}{r^2}\right], \tag{4}$$

and

$$\frac{\partial^2 \psi}{\partial z^2} + \frac{\partial^2 \psi}{\partial r^2} - \frac{1}{r}\frac{\partial \psi}{\partial r} = -r\eta, \tag{5}$$

where

$$Re = \frac{\Omega R^2}{\nu},$$

and

$$J = \frac{\partial \psi}{\partial z}\frac{\partial}{\partial r} - \frac{\partial \psi}{\partial r}\frac{\partial}{\partial z}.$$

The boundary conditions relevant to the experiments of Escudier (1984) to complete

the system (3)-(5) are:

$$\begin{aligned}
\psi = v = \eta = 0 \qquad & (r = 0, \quad 0 \le z \le H/R), \\
\psi = v = 0, \quad \eta = -\frac{1}{r}\frac{\partial^2 \psi}{\partial r^2} \qquad & (r = 1, \quad 0 \le z \le H/R), \\
\psi = 0, \quad v = r, \quad \eta = -\frac{1}{r}\frac{\partial^2 \psi}{\partial z^2} \qquad & (z = 0, \quad 0 \le r \le 1), \\
\psi = v = 0, \quad \eta = -\frac{1}{r}\frac{\partial^2 \psi}{\partial z^2} \qquad & (z = H/R, \quad 0 \le r \le 1).
\end{aligned} \tag{6}$$

The boundary condition at $r = 0$ is due to the axial symmetry of the flow, the boundaries at $z = H/R$ and $r = 1$ are rigid and stationary, while at $z = 0$, the rigid endwall is in constant rotation for $t > 0$. The fluid is stationary for $t \le 0$.

3. Method of Solution

The system of differential equations (3) – (5) is replaced by an approximating set of finite-difference equations, defined on a uniform mesh in the r, z plane at times $n\Delta t$ $(n = 0, 1, 2, ...)$. There are $(nr + 1) \times (nz + 1)$ grid nodes, and in all the cases presented here, the increments Δr and Δz are equal. Second-order accurate centered differences are used to approximate all the spatial derivatives except those in the advection terms, where the Jacobian conserving difference operator J is approximated using a scheme due to Arakawa (1966). The time-differencing scheme used is that of Miller & Pearce (1974) which consists of alternate timesteps. For a prediction equation of the form $\partial F/\partial t = G(F)$, the odd time-steps are advanced according to

$$F^* = F^n + \Delta t G(F^n),$$

$$F^{n+1} = F^n + \Delta t G(F^*),$$

while for even time-steps

$$F^{n+1} = F^n + \Delta t G(F^n).$$

The prognostic equation (5) for the streamfunction is solved using the generalized cyclic reduction method of Sweet (1974).

To implement the boundary conditions for the azimuthal vorticity at the solid boundaries at time $(n + 1)\Delta t$, the streamfunction field at that time is needed. This is achieved by the following algorithm. First, the prediction equations (3) and (4) for v and η may be advanced to the next time-step $(n + 1)\Delta t$ for the interior points since the prognostic equation (5) for ψ only requires knowledge of the interior values of η. From the solution to (5) together with the boundary conditions for ψ, the streamfunction is known everywhere at $t = (n + 1)\Delta t$. The boundary values of η can now be estimated from ψ by noting that ψ and its normal derivative vanish at a rigid boundary. Hence, expanding ψ about the first point in from the boundary leads to

$$\eta(nr + 1, j) = -2\psi(nr, j)/\Delta r^2,$$

$$\eta(i, 1) = -2\psi(i, 2)/(r\Delta z^2),$$

and

$$\eta(i, nz + 1) = -2\psi(i, nz)/(r\Delta z^2).$$

Proper resolution of the boundary layers and any recirculation zones was ensured by the use of $\Delta r = \Delta z = 1/60$. A number of runs for $H/R = 1.5$ were performed using $\Delta r = \Delta z = 1/40$ with only slight differences in the outline of the recirculation zone being noted — the positions of the stagnation points were not appreciably altered by the reduction in resolution. One run at $H/R = 2.5$ and $Re = 2126$ implemented $\Delta r = \Delta z = 1/100$. The difference between the streamlines from these results and those from calculations with $\Delta r = \Delta z = 1/60$ were insignificant. All the calculations presented here are for $\Delta r = \Delta z = 1/60$ and $\Delta t = 0.05$, except for the one case of $H/R = 2.5$ and $Re = 2126$ where $\Delta r = \Delta z = 1/100$ and $\Delta t = 0.025$. In all cases, the stability of the model was ensured by the time-step satisfying both the Courant-Friedrichs-Lewy condition and the diffusion requirement (Williams 1967),

$$\Delta t < \frac{1}{8} Re \Delta r^2.$$

The quality of the numerical computations was further verified by (i) direct comparisons with experimental results (§4), and by (ii) evaluation of the vorticity integral (Dijkstra & van Heijst 1983). From the definition of the azimuthal vorticity (2), together with the boundary conditions, the streamfunction and its normal derivatives vanish on solid boundaries and $\psi = 0$ on the axis of symmetry, hence

$$\int\int\int_V r\eta dV = 2\pi \int_{r=0}^{1} \int_{z=0}^{H/R} r^2 \eta dz dr = 0. \tag{7}$$

At $t = 1000$, this integral was evaluated by means of a two-dimensional trapezoidal rule, and the positive and negative contributions to the trapezoidal sum accumulated separately in $I(\eta^+)$ and $I(\eta^-)$ respectively. In the limit $\Delta r, \Delta z \to 0$, $I(\eta^+) + I(\eta^-) = 0$. The degree to which this is achieved is an indication of the quality of the numerical scheme. Table 1 lists the values of the integral (7) together with $I(\eta^+)$ and $I(\eta^-)$ for a selection of the cases considered. It is clear that the accuracy of the calculations is improved by increasing the resolution from $\Delta r, \Delta z = 1/40$ to $1/60$. For the case $Re = 1256$, $I_{rel} = (I(\eta^-) + I(\eta^+))/(I(\eta^-) - I(\eta^+)) \simeq 0.0015$ when $\Delta r, \Delta z = 1/40$, whereas $I_{rel} \simeq 0.00069$ for $\Delta r, \Delta z = 1/60$. On further grid refinement, as illustrated by the $Re = 2126$ case, $I_{rel} \simeq 0.00077$ for $\Delta r, \Delta z = 1/60$ and $I_{rel} \simeq 0.00055$ for $\Delta r, \Delta z = 1/100$, indicating that $\Delta r, \Delta z = 1/60$ constitutes a good compromise between the level of accuracy and the computational effort required to achieve it. The extent to which the vorticity integral (7) is satisfied is reduced as Re is increased. However, in the

Re range considered, this trend is very weak, as when $Re = 1492$ and Δr, $\Delta z = 1/60$, $I_{rel} \simeq 0.00072$, whereas for $Re = 3023$ and Δr, $\Delta z = 1/60$, $I_{rel} \simeq 0.00078$.

Although most of the solutions presented in this study reach a steady state (those which do not are noted), it is important to ensure that the model has temporal as well as spatial accurracy. In the parameter range where the flow reaches a steady state, Escudier (1984) reported that the time taken to reach this steady state from an impulsive start was typically tens of seconds. In that same parameter range, i.e. $1.5 \leq H/R \leq 2.0$ and $1000 \leq Re \leq 1500$, the numerical model reaches steady state for t between 500 and 700. In the case where $\nu = 4.5 \times 10^{-5} m^2/s$ and $R = 9.5 \times 10^{-2} m$, which are the values in the experiments of Escudier (1984), we find $\Omega \simeq Re/200$ and a 'spin-up' time to steady state of approximately 60 seconds. The numerical result is consistent with the experimental observations.

Escudier found experimentally that the flow undergoes a transition to unsteadiness at some critical combinations of Re and H/R and he has mapped out this transition (Figure 1). At the point where the flow becomes unsteady, the flow visualization technique is no longer able to give a clear picture of the flow characteristics. The present numerical solutions are found to accurately predict those flows which lead to a steady state. This has given us confidence to investigate the transition to unsteadiness and this aspect of the flow is the subject of a further report which is in preparation.

4. Results and Discussion

Escudier (1984) has mapped out a stability diagram in the $(Re, H/R)$ plane delineating the regions where single, double and triple recirculation zones occur, together with the boundary between steady and oscillatory flows. This diagram is reproduced in Figure 1. The parameter values at which the flow has been simulated in this study are also indicated in this figure. Escudier has made available photographs of the recirculation zones and a number of these are reproduced here for comparison with the numerical solutions. The reader should be aware that in the photographs of the experiment, radial distances are reported to appear uniformly stretched by 8% due to refraction at the various interfaces.

The following is a brief description of the basic flow features.

The fluid, which completely fills the cylindrical container, is initially at rest. At $t = 0$, the bottom endwall is impulsively set to rotate at constant angular speed Ω. An Ekman boundary layer develops on the rotating disk with thickness of order $(\nu/\Omega R^2)^{0.5}$. This rotating boundary layer then acts as a centrifugal pump, sending fluid radially outwards in a spiralling motion while 'sucking' fluid into it from above. This pumping action of the boundary layer together with the presence of the cylindrical wall at $r = R$ sets up a secondary meridional circulation. The fluid pumped out of the Ekman layer spirals up the cylindrical wall establishing a Stewartson-type boundary layer (see Greenspan 1968). In time, fluid with angular momentum reaches the vicinity of the stationary top endwall, where it is turned and advected towards the centre. It spirals inwards creating a further boundary layer on the top endwall. On the endwall the fluid separates at $r = 0$ and a concentrated central vortex is formed whose core size depends on the depth of the boundary layer from which it emerged. The fluid then spirals down this central vortex to be sucked back into the Ekman layer.

The experimental studies of this flow show that it undergoes a series of bifurcations as the two governing parameters, Re and H/R, are varied. The present study focusses on the development of the flow characteristics with Re and H/R up to the point where the flow no longer reaches a steady state. In particular, in the region of parameter space considered, i.e. $Re \leq 3000$ and $H/R \leq 3.5$, the flow is observed experimentally to remain axisymmetric and laminar, and for the most part to reach a steady state.

Figure 1 suggests that the flow characteristics depend critically on the Reynolds number. The numerical solutions show, however, that the basic dynamics of the central

vortex are inertially driven and that viscous shears are negligible outside recirculation zones, boundary layers and away from the meridional shear layer in the bottom half of the cylinder which is caused by the strong turning at the corner $r = R$, $z = 0$. A comparison of the 'streamline' contours, i.e. intersections of stream surfaces with the meridional plane, and contours of the angular momentum $\Gamma = rv$, on the meridional plane show that even at the relatively low value of $Re = 1000$ (see Figure 2a) Γ is constant, to high order, on streamlines outside boundary layers. At this value of Re, the curvature of the streamlines of the vortical fluid returning towards the lower rotating endwall does not change sign and the secondary meridional flow consists of a simple overturning motion. From the contour plots of the azimuthal vorticity (Figure 2a(iii)). we find that η is positive in the boundary layer regions and negative in the interior flow, consistent with a deceleration of the meridional flow in the boundary layers. Of particular interest, one should note the small region of positive η just above the Ekman layer about the axis of symmetry.

It is interesting to examine the effect of increasing Re for the case in which $H/R = 2.5$. At $Re = 1600$ a waviness is evident in the streamtubes of the central vortex as well as in the contours of Γ (see Figure 2b). Comparing the Γ contours of the two cases $Re = 1000$ and $Re = 1600$, it is clear that a greater proportion of the fluid's angular momentum has been advected towards $r = 0$, in the upper boundary layer region. leading to the formation of what appears to be a weak centrifugal wave in the higher Re case. The contours of η at $Re = 1600$ (see Figure 2b(iii)) are qualitatively similar to those at $Re = 1000$, but now the extrema in the values of the azimuthal vorticity have increased. The region of positive azimuthal vorticity in the interior of the flow is extended considerably and roughly coincides with the region of 'wavy' streamtubes.

The above effects are further enhanced as Re is increased to 1800. Here the streamtubes (Figure 2c) clearly indicate the presence of a centrifugal wave with two periods and two bulges on the axis at approximately 1/3 and 2/3 of H/R. Note however that the central vortex, as it emerges from the endwall boundary layer has streamtubes which are almost parallel with a relatively large radial gradient, indicating the presence of a relatively large axial velocity in this core flow.

An increase in Re to 1918 crosses the boundary between no 'breakdowns' and 1 - 2 'breakdowns' on Figure 1. The amplitude of the waves has increased and their wavelength decreased (see Figure 2d). With the increased amplitude and decreased

wavelength, the associated axial deceleration is large enough to cause the flow to stagnate under the crest of the wave. Within this stagnant region is found a near spherical region of recirculating fluid which is termed a vortex breakdown bubble, i.e. a toroidal vortex centered on the axis of a columnar vortex. At this particular value of H/R there are two breakdown bubbles, the downstream bubble being considerably smaller and the recirculating flow within it slower than in the leading bubble.

For $H/R < 1.95$, both the experimental investigations of Escudier (1984) and our numerical calculations only identify single breakdown bubbles and for $H/R < 1.2$, no breakdown bubbles are found. Pao (1970) observed, in a related problem where the cylinder wall also rotates at the same angular speed as the disk, that for $H/R = 1.0$ and $Re > 500$ standing waves appear in the axial plane and reported a similar dependence on Re for these waves as is found in this study. His experimental investigations include cases up to $Re = 8600$ where the flow was reported to be steady, axisymmetric and laminar. However, he did not find any recirculating breakdown bubbles in his low aspect ratio ($H/R = 1.0$) container.

As Re is increased to 1942 (Figure 2e), 1996 (Figure 2f) and 2126 (Figure 2g), very good agreement is found between the calculated stream surfaces and the observations of Escudier (1984). Some of these experimental observations are included for comparison with the numerical solutions in Figure 3.

Although the length of the recirculation bubbles has grown larger with the increases in Re, the wavelength of the wavy disturbance on the outer streamtubes has been reduced. There remains a general trend that as Re is increased, the wavelength is reduced and the wave amplitude increased. The increase in the bubble diameters with Re is indicative of the increased wave amplitudes. The shortening of the wavelength is also consistent with the behaviour of the recirculation bubbles. As Re is increased, the region of near parallel flow just after the vortex emerges from the boundary layer on the stationary endwall is shortened. This leads to a migration of the leading bubble towards this endwall. Note also that the distance between the two bubbles is progressively reduced as Re is increased.

The distribution of Γ is particularly interesting. For fluid in the central vortex that has emerged from the upper boundary layer, Γ is conserved on the streamtubes for some axial distance over which the vortex remains concentrated. As the fluid spirals downstream past the breakdown region, there is a change in the angular momentum.

When the fluid is first deflected radially outwards around the breakdown bubble, there is an increase in Γ and when it is converged again around the downstream half of the bubble it loses some of this gain in angular momentum. The gradients in azimuthal velocity are large enough for the viscous stresses to effect these changes. Past the breakdown regions, the angular momentum distribution then corresponds to essentially solid body rotation of the fluid. In essence, in these flows, the breakdown region is like a transition region from a concentrated vortical flow to solid body rotation.

The details of the flow structure in the recirculation bubble are of particular interest in this study, even though their dynamical significance to the overall flow structure is quite secondary. The main reason for this interest is that they provide an excellent test for the accurracy of the numerical solutions. It is possible to obtain very good flow visualizations of the breakdown bubbles and their structure, and correspondingly of critical points and flow reversals. These features are much more demanding on a numerical model than the relatively simple structure of the outer flow.

Comparing in detail the structure of the recirculation regions as determined numerically and observed experimentally for $Re = 2126$ and $H/R = 2.5$ we find very good agreement between the two. The structure of the upstream bubble is now clearly interpreted with the aid of the numerical streamlines. The leading stagnation point is well defined in the flow visualization, however the downstream stagnation point is not as some dye finds its way into the bubble and some is swept past. Note that the leading dye streak is very thin - this is also reflected in the calculated streamlines which are very close together in the approach flow to the stagnation point. As the fluid passes over the bubble at maximum diameter, the streamlines indicate a local acceleration of the meridional flow over the 'obstacle', i.e. bubble. As the fluid passes the bubble, it converges back towards the axis, however the axial flow is now considerably slower than it was in its approach to the leading stagnation point. This is seen in the increased distance between the calculated streamlines as well as in the much broadened dyestreak. The dye photograph of the leading bubble shows a thin well defined outer envelop with a rather broad, diffuse inner core. This is matched by the computed streamlines where they are contracted to the outer edge of the bubble and spread out within the interior. As for the downstream bubble, a similar situation is found. This information is not evident from the dye photograph since it appears that the dye is residing principally between a narrow band of streamlines which envelop the bubble, with virtually no dye

inside the bubble. The computed streamlines indicate that the recirculating flow in the downstream bubble is considerably slower than in the upstream bubble. Downstream of the second bubble, the enveloping dyestreak is broad and is tapered as it approaches the Ekman layer. This behaviour is mirrored in the computed streamlines and may be interpreted as an axial acceleration of the flow, probably as a result of the boundary layer suction.

This very close agreement between experimental observation and numerical calculation of the recirculation zones has not been achieved in every case, although in all cases the agreement has been very good. The reason is because the structure of the recirculation zones in the vicinity of parameter space where a recirculation zone just emerges is critically dependent on the value of Re. For example, the small change in Re from 1918 to 1942 (1.2%) results in a 25% increase in the diameter of the leading bubble and a 300% increase in the diameter of the second bubble, whereas the outer flow remains virtually unchanged. Hence, a small percentage error in the estimate of Re can be responsible for a significant difference between the observed structure of the recirculation bubbles and their computed structure. Unfortunately, no uncertainty estimates on Re are available for the experimental observations. Escudier reports, however, that the temperature of the fluid was maintained at $25°C \pm 0.1°C$ and the viscosity of the fluid varied by about 5% per °C. Hence a possible uncertainty of 0.5% exists in the estimate of Re due to the uncertainty in viscosity alone. For flows that are not so close to these critical parameter regions, the structure of the recirculation bubbles is not so variable with Re and a much closer agreement between the computations and the observations was found.

As the Reynolds number of the flow increases, the downstream bubble approaches the tail end of the upstream bubble. Just beyond the value of Re at which the tail stagnation point of the upstream bubble coincides with the leading stagnation point of the downstream bubble, the flow bifurcates. This bifurcation leads to a flow in which there are two stagnation points on the axis of symmetry defining the head and tail of the recirculation zone which encloses two distinct zones. These two zones are connected by a ring seen as two saddle-points either side of the axis of symmetry in the meridional plane. In the case of $Re = 2494$, $H/R = 2.5$ (see Figure 2h), this flow pattern is steady. The two critical streamlines, i.e. $\psi = 0$ enclosing the bubble and $\psi = 1.609 \times 10^{-6}$ defining the saddle-points, are very close together around the outer envelope of the recirculation bubble, whereas there is a considerable gap between them near the axis of symmetry.

This is also reflected in the dye photograph (see Figure 3b) where the dye depicting the outer shell of the bubble is a thin well defined shell, while it is broad and diffuse in the inner core. Also, in the vicinity of the saddle-points, the dye lines are confused and it is difficult to resolve the flow from them.

When Re is increased to 2765, the computed flow is unsteady and its structure oscillates between the structures typical of $Re = 2126$ and $Re = 2494$. Figure 2i shows time-averages of ψ, Γ and η. The development of this unsteadiness and its periodicity is the subject of further study. Note, however, that the outline of the head of the upstream recirculation zone and the outline of the internal downstream recirculation zone shown in the 'snap-shot' of the experimental flow (Figure 3c, found by Escudier (1984) to be steadily oscillating) are well represented by the time-averaged computed streamlines. This suggests that the dye-lines of the unsteady flow retain some information about the time history of the flow.

The flow develops into three distinct zones for $Re > 2680$ when $H/R = 3.25$ and $Re > 3000$ for $H/R = 3.5$. In all cases considered, the two downstream recirculation zones merge and result in a flow pattern similar to that described earlier for $H/R = 2.5$ and $Re = 2494$. The upstream breakdown region however remains separate and its flow structure is as described for the upstream bubble when $H/R = 2.5$ and $Re = 2126$. The numerical solutions for this triple breakdown did not reach steady state after $t = 1000$, which corresponds to 20,000 time steps. In real time, this is equivalent to integrating the system of governing equations, from rest, for approximately 70 seconds for the corresponding experimental values of Escudier (1984). The parameter values for which these solutions were obtained are very near those delineating the unsteady flow regions according to the stability diagram (Figure 1), where it was observed experimentally that steady conditions are reached in a very long time, longer than 10's of seconds. Perhaps if the integrations were carried out for longer times they would indeed reach steady state. The oscillations for $H/R = 3.25$ are almost undetectable, consisting of oscillations of approximately 1% in the values of the streamfunction. The oscillations found in the solutions for $H/R = 3.5$ were considerably larger, with the middle breakdown zone oscillating most. The upstream breakdown bubble is close to steady state, and the tail end of the downstream breakdown region is also varying very slowly. Figure 4 are time-averaged contours of ψ, Γ and η for $Re = 3061$ and $H/R = 3.5$, which are to be compared with Figure 5 which is a photograph of the flow for the same values of

the parameters. It is interesting to note Escudier's (1984) observation that the central recirculation zones for the $H/R = 3.5$ cases never develop into well defined regions, and this now appears to be due to these regions never quite reaching steady state.

5. Conclusion

A numerical solution of the axisymmetric Navier-Stokes equations has been obtained and used to examine the vortex breakdown phenomenon which occurs at certain values of the governing parameters for flows in an enclosed cylinder driven by a rotating endwall. The accuracy of the numerical solutions has been established by varying the grid resolution and satisfying an integral identity which exists for the flow. The numerical solutions are compared extensively with available experimental results, particularly dye-streak photographs of the flow, mostly at steady state. The extent of the agreement between the numerical solutions and the experimental results is critically examined and is found to be very good. Certain features which were not fully resolved by the experiments have now been given plausible explanations from the numerical results. The numerical solutions also provide a clear picture of the topology of the flow, especially of the structure of the multiple breakdown zones.

In part II of this study, the numerical solutions are examined further and a physical understanding of the vortex breakdown phenomenom is gained.

The scene is also set for future studies in the unsteady regime. Unsteady flows are generally less amenable to study by flow visualization techniques as relationships between unsteady pathlines, streamlines and streaklines are not straightforward. The interpretation of streaklines from flow visualization results for example, requires more care. For the time-dependent numerical model presented here, these distinctions are more readily made and the interpretation of the flow characteristics more tractable. However, in extending the present axisymmetric model into the unsteady regime the assumption of axial symmetry is in question where there are no experimental results to support it. It is not expected to be valid as the flows become increasingly oscillatory and unstable as Re and H/R are increased.

REFERENCES

Arakawa, A. 1966 Computational design for long-term numerical integration of the equations of fluid motion: Two-dimensional incompressible flow. Part 1. *J. Comp. Phys.* **1**, 119–143.

Dijkstra, D. & van Heijst, G. J. F. 1983 The flow between two finite rotating disks enclosed by a cylinder. *J. Fluid Mech.* **128**, 123–154.

Escudier, M. P. 1984 Observations of the flow produced in a cylindrical container by a rotating endwall. *Experiments in Fluids* **2**, 189–196.

Escudier, M. P. & Keller, J. J. 1983 Vortex breakdown : A two-stage transition. *AGARD CP*-342.

Escudier, M. P. & Zehnder, N. 1982 Vortex flow regimes. *J. Fluid Mech.* **115**, 105–121.

Faler, J. H. & Leibovich, S. 1978 An experimental map of the internal structure of a vortex breakdown. *J. Fluid Mech.* **86**, 313–335.

Greenspan, H. P. 1968 The theory of rotating fluids. *(Cambridge Univ. Press).*

Harvey, J. K. 1960 Analysis of the 'vortex breakdown' phenomenon, Part 2. *Imp. College, Aero. Dept. Rep. No.* 103.

Lugt, H. J. & Abboud, M. 1987 Axisymmetric vortex breakdown with and without temperature effects in a container with a rotating lid. *J. Fluid Mech.* **179**, 179–200.

Lugt, H. J. & Haussling, H. J. 1973 Development of flow circulation in a rotating tank. *Acta Mechanica* **18**, 255–272.

Lugt, H. J. & Haussling, H. J. 1982 Axisymmetric vortex breakdown in rotating fluid within a container. *J. App. Mech.* **49**, 921–923.

Miller, M. J. & Pearce, R. P. 1974 A three-dimensional primitive equation model of cumulonimbus convection. *Quart. J. R. Met. Soc.* **100**, 133-154.

Pao, H.-P. 1970 A numerical computation of a confined rotating flow. *J. App. Mech.* **37**, 480–487.

Peckham, D. H. & Atkinson, S. 1957 Preliminary results of low speed wind tunnel tests on a Gothic wing of aspect ratio 1.0. *Aero. Res. Counc. CP*-508.

Ronnenberg, B. 1977 Ein selbstjustierendes 3-KomponentenLaserdoppleranemometer nach dem Vergleichsstrahlverfahren, angewandt für Untersuchungen in einer stationären zylindersymmetrischen Drehströmung mit einen Rück-

stromgebiet. *Max-Planck-Inst. Bericht* 20.

Sarpkaya, T. 1971 On stationary travelling vortex breakdown. *J. Fluid Mech.* **45**, 545–592.

Sweet, R. A. 1974 A generalized cyclic reduction algorithm. *SIAM J. Numer. Anal.* **10**, 506–520.

Vogel, H. U. 1968 Experimentelle Ergebnisse über die laminare Strömung in einen zylindrischen Gehäuse mit darin rotierender Scheibe. *Max-Planck-Inst. Bericht* 6.

Williams, G. P. 1967 Thermal convection in a rotating fluid annulus: Part 1. The basic axisymmetric flow. *J. Atmos. Sci.* **24**, 144–161.

Re	H/R	nr	nz	$I(\eta)$	$I(\eta^+)$	$I(\eta^-)$
1256	1.5	40	60	-.000386	.12590	-.12628
1256	1.5	60	90	-.000175	.12619	-.12637
1492	1.5	40	60	-.000418	.12888	-.12929
1492	1.5	60	90	-.000188	.12908	-.12927
1854	1.5	40	60	-.000461	.13130	-.13176
1854	1.5	60	90	-.000206	.13417	-.13438
1994	2.5	60	150	-.000237	.15684	-.15708
2126	2.5	60	150	-.000244	.15893	-.15918
2126	2.5	100	250	-.000175	.16041	-.16058
2889	3.5	60	210	-.000277	.18056	-.18083
3023	3.5	60	210	-.000286	.18206	-.18234

TABLE 1: CHARACTERISTICS OF THE VORTICITY INTEGRAL (7) FOR SELECTED CASES.

FIGURE 1: STABILITY BOUNDARIES FOR SINGLE, DOUBLE AND TRIPLE BREAKDOWNS, AND BOUNDARY BETWEEN STEADY AND OSCILLATORY FLOW, IN THE (*Re, H/R*) PLANE (EMPIRICALLY DETERMINED BY ESCUDIER (1984)). THE LOCATIONS IN PARAMETER SPACE WHERE THE FLOW HAS BEEN SIMULATED ARE INDICATED BY □.

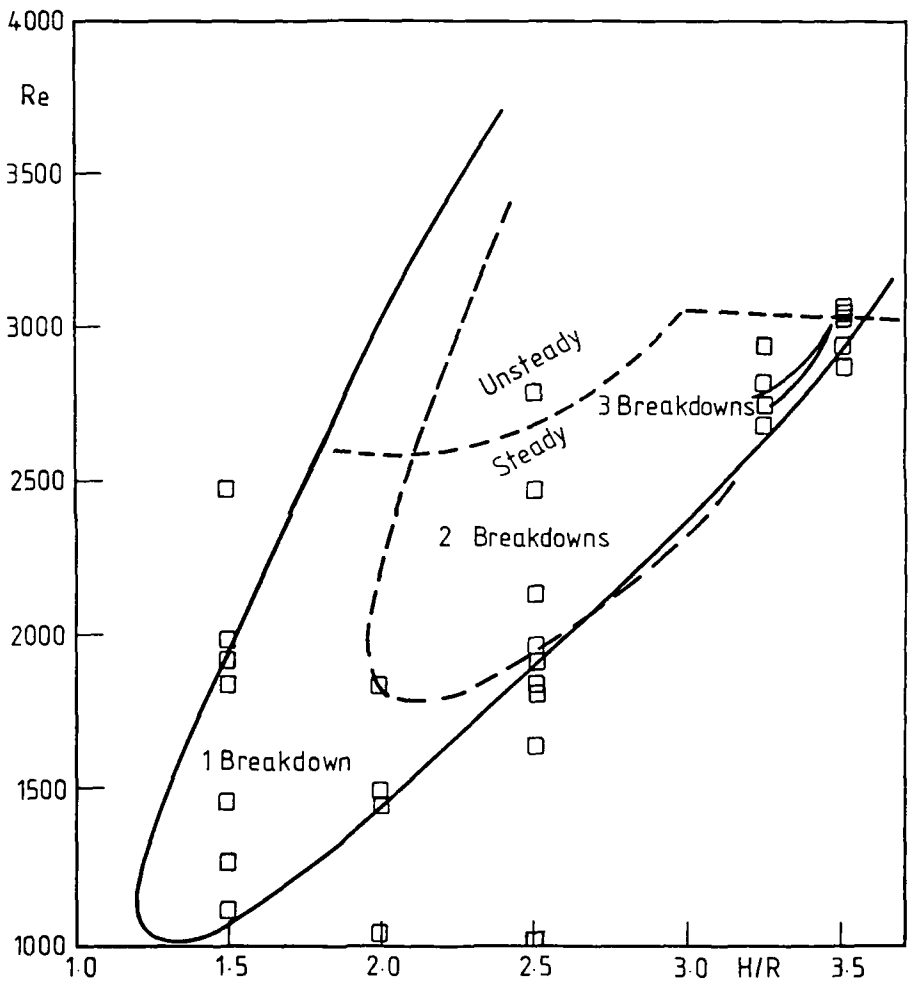
4000
Re
3500
3000
2500
2000
1500
1000
1·0
1·5
2·0
2·5
3·0
H/R
3·5
Unsteady
Steady
3 Breakdowns
2 Breakdowns
1 Breakdown

FIGURE 1

FIGURE 2: CONTOURS OF (i) ψ, (ii) Γ AND (iii) η IN THE MERIDIONAL PLANE FOR H/R = 2.5 AND *Re* AS INDICATED. THE CONTOUR LEVELS ARE NON-UNIFORMLY SPACED, WITH 20 POSITIVE AND 20 NEGATIVE LEVELS DETERMINED BY CONTOURLEVEL(i) = MAX(*variable*) × $(i/20)^3$ AND CONTOURLEVEL(i) = MIN(*variable*) × $(i/20)^3$ RESPECTIVELY. ALL ARE PLOTTED AT t = 1000 BY WHICH TIME STEADY STATE FLOW CONDITIONS HAVE BEEN REACHED, EXCEPT FOR (i) WHICH SHOWS THE TIME AVERAGES OVER $750 \leq t \leq 1000$ OF AN OSCILLATORY FLOW.

(i) Ψ: Re = 1000, H/R = 2.5

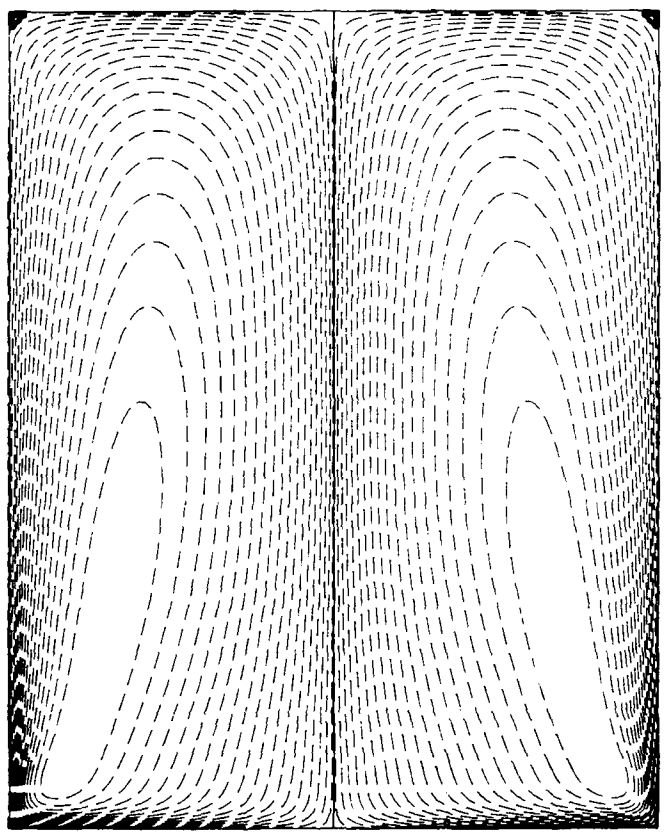

min. = -9.7×10^{-3} max. = 1.6×10^{-7}

FIGURE 2a (i)

(ii) Γ: Re = 1000, H/R = 2.5

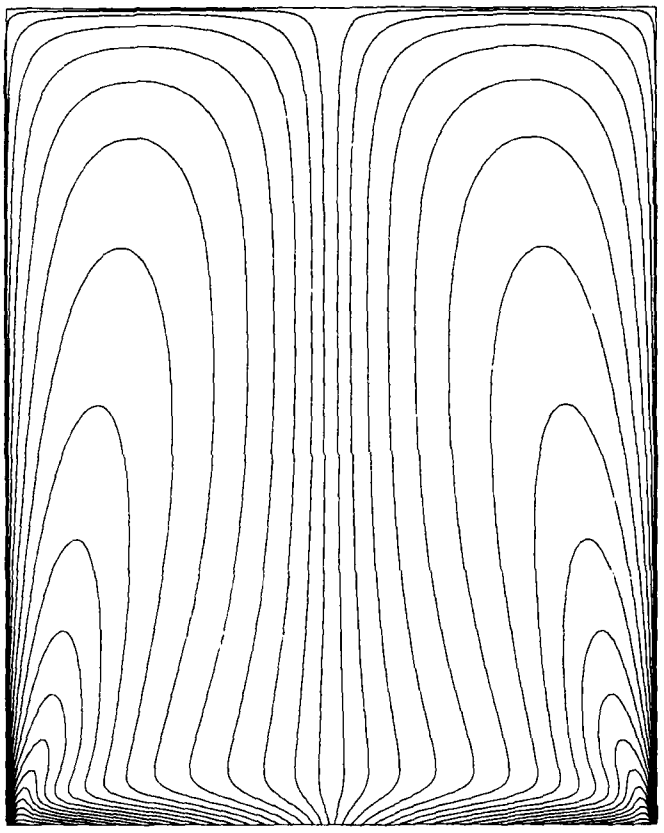

min. = 0 max. = 1.0

FIGURE 2a (ii)

(iii) η: Re = 1000 H/R = 2.5

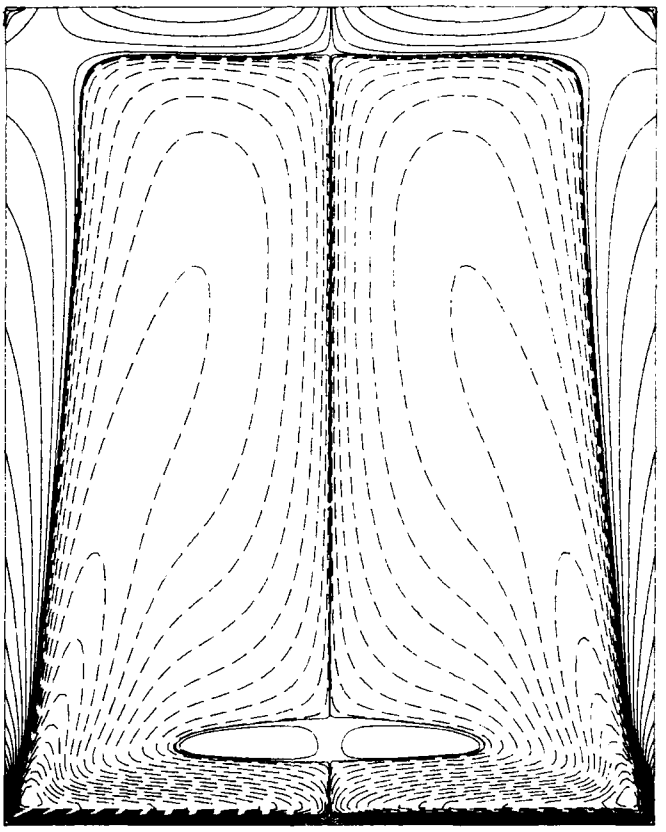

min. = -2.8 max. = 11.6

FIGURE 2a (iii)

(i) Ψ Re = 1600 H/R = 2.5

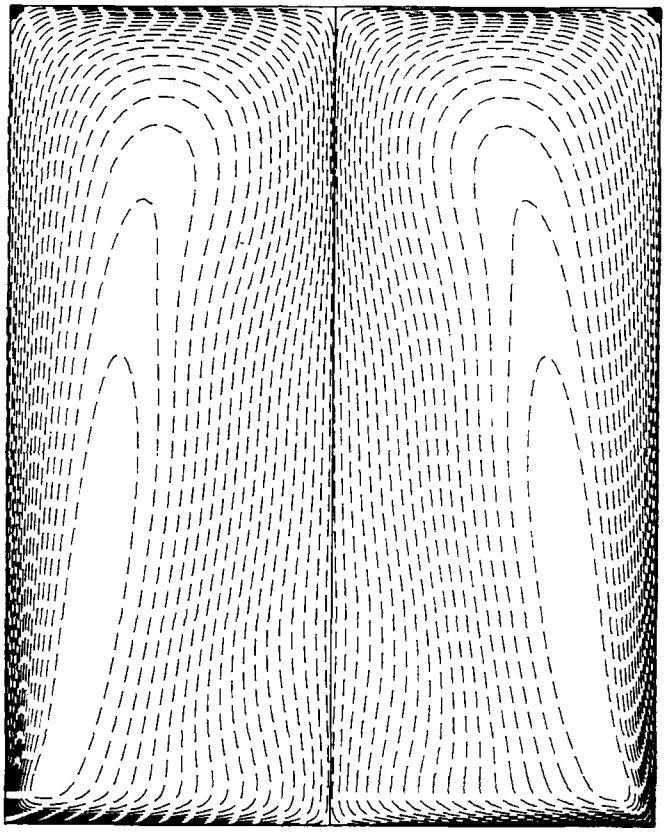

min. = -8.3×10^{-3} max. = 2.1×10^{-7}

FIGURE 2b (i)

(ii) Γ: Re = 1600 H/R = 2.5

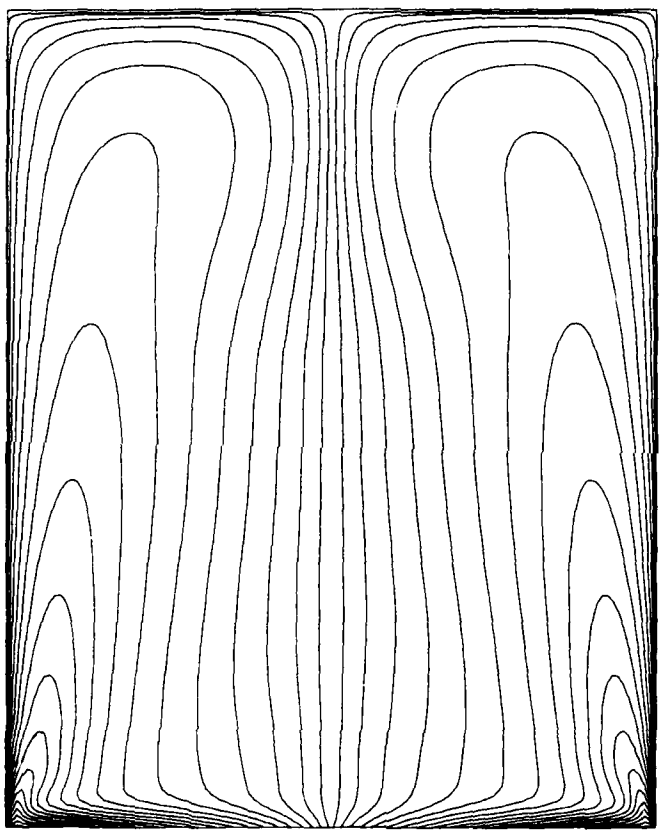

min. = 0 max. = 1.0

FIGURE 2b (ii)

(iii) η: Re = 1600 H/R = 2.5

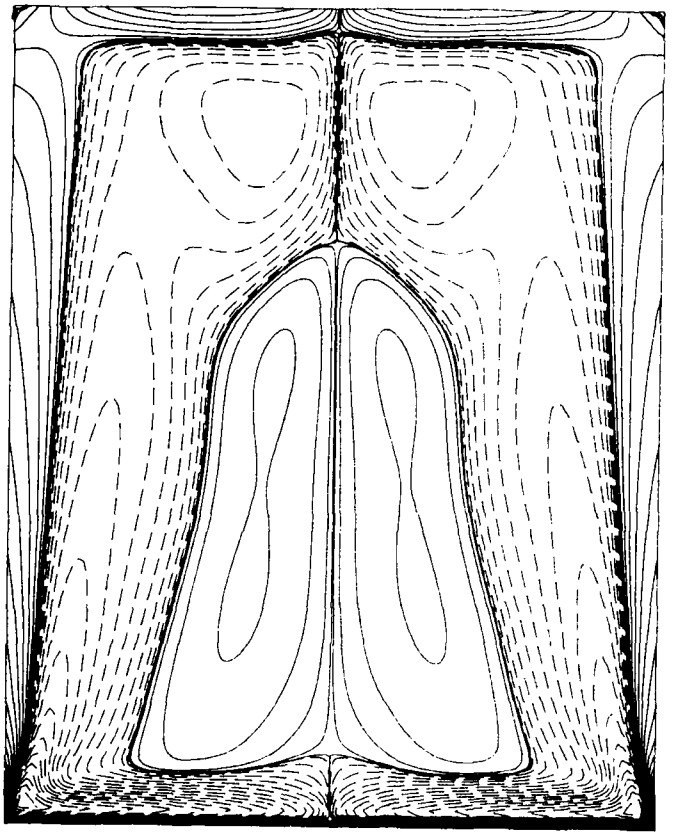

min. = -3.5 max. = 14.4

FIGURE 2b (iii)

(i) Ψ: Re = 1800 H/R = 2.5

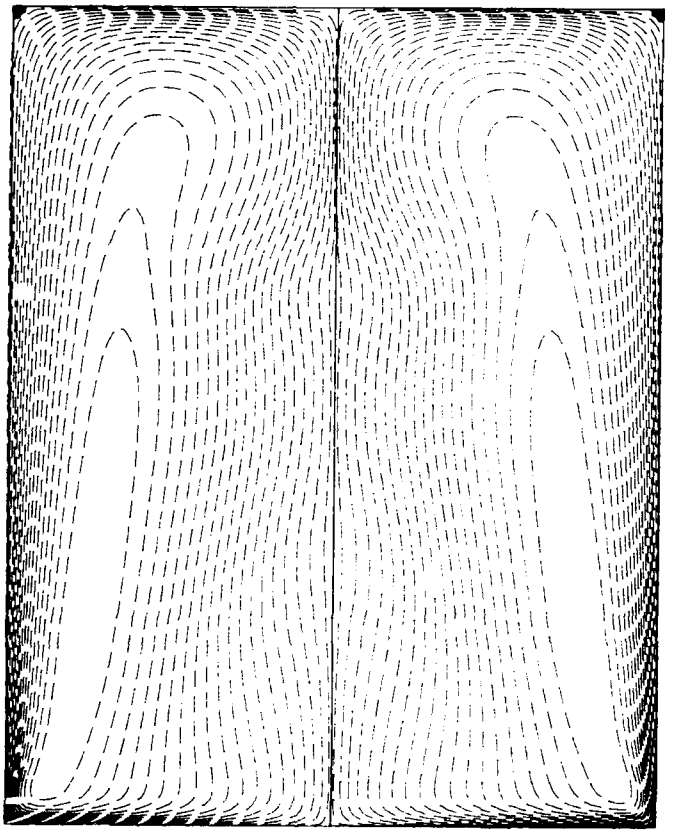

min. = -8.0×10^{-3} max. = 2.4×10^{-7}

FIGURE 2c (i)

(ii) Γ: Re = 1800 H/R = 2.5

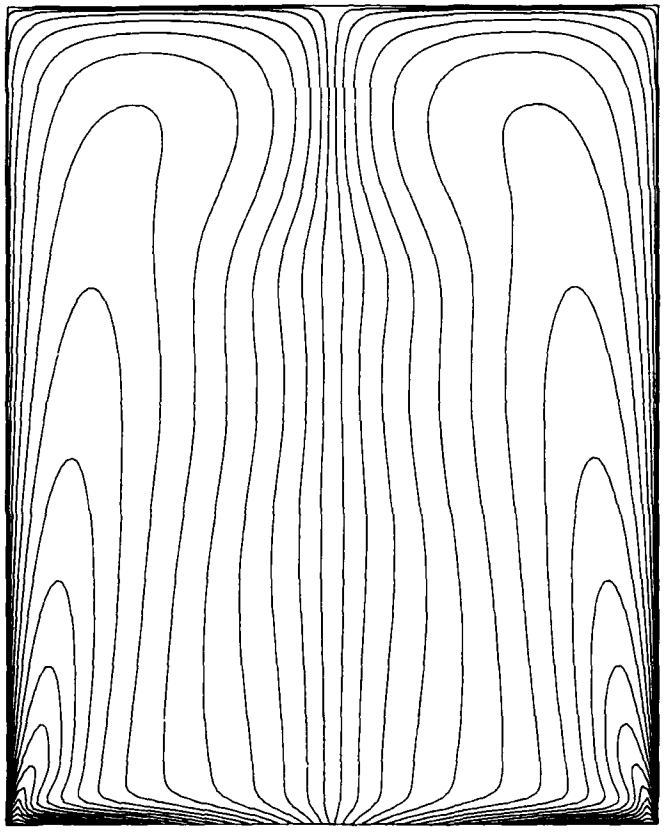

min. = 0 max. = 1.0

FIGURE 2c (ii)

(iii) η: Re = 1800 H/R = 2.5

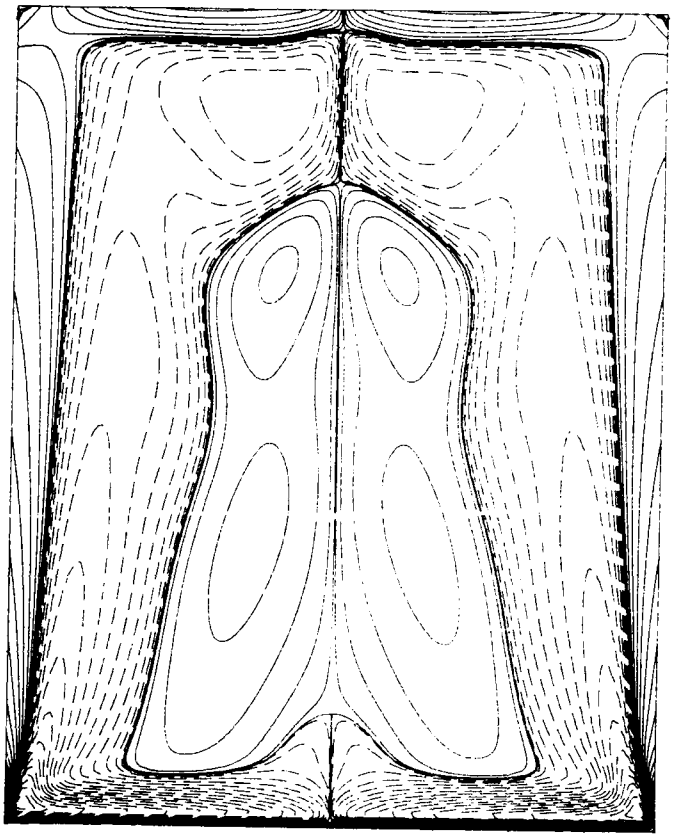

min. = -3.7 max. = 15.2

FIGURE 2c (iii)

(i) Ψ: Re = 1918 H/R = 2.5

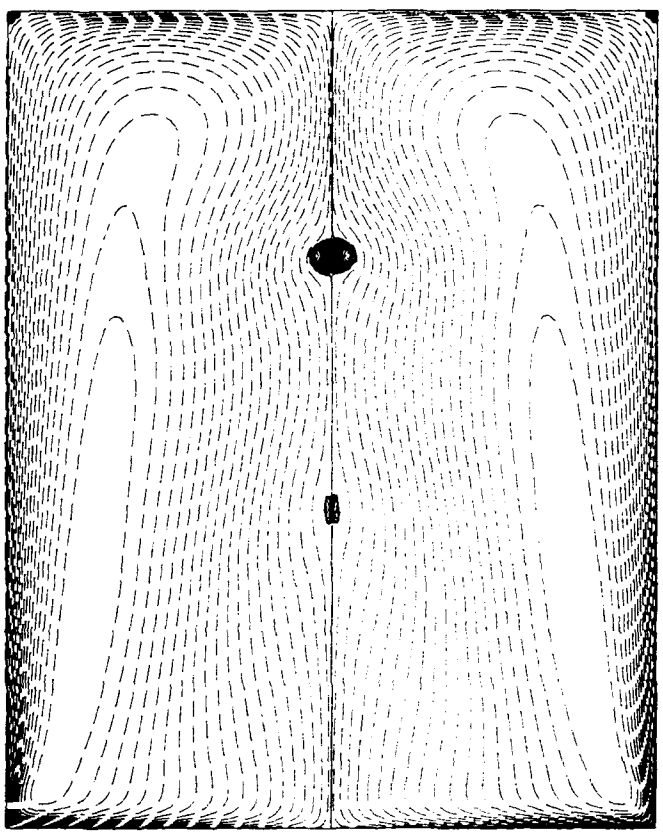

min. = -7.9×10^{-3} max. = 1.0×10^{-6}

FIGURE 2d (i)

(ii) Γ: Re = 1918 H/R = 2.5

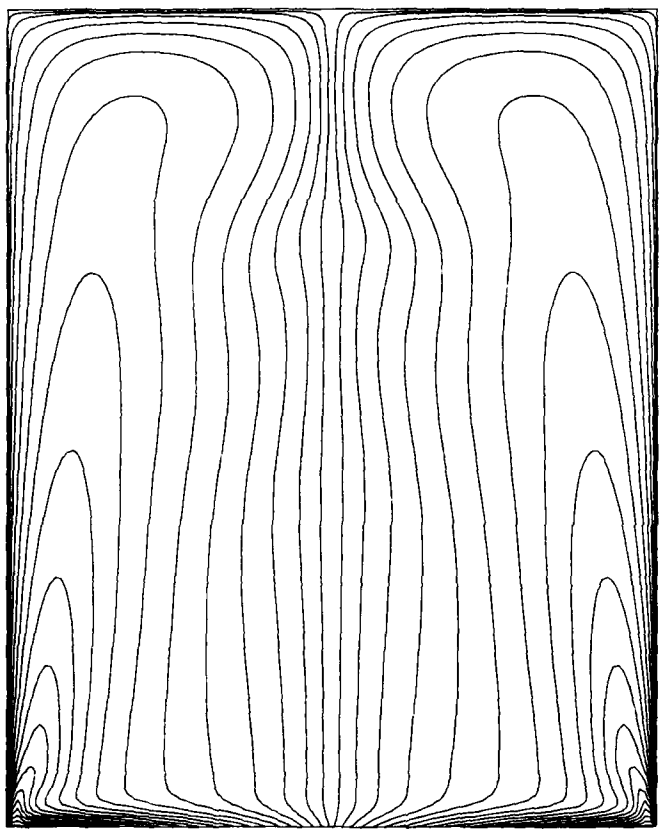

min. = 0 max. = 1.0

FIGURE 2d (ii)

(iii) η: Re = 1918 H/R = 2.5

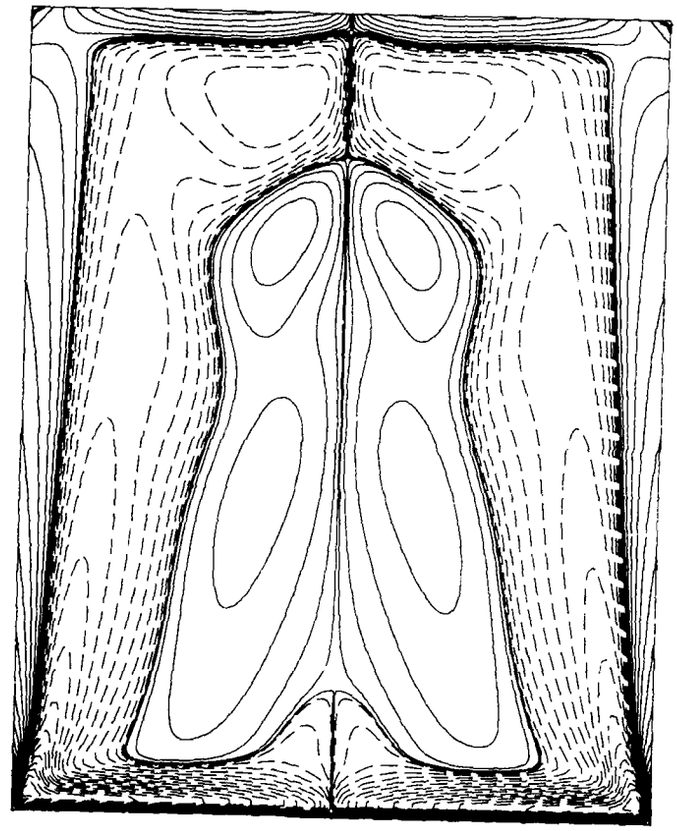

min. = -3.8 max. = 15.6

FIGURE 2d (iii)

(i) Ψ: Re = 1942 H/R = 2.5

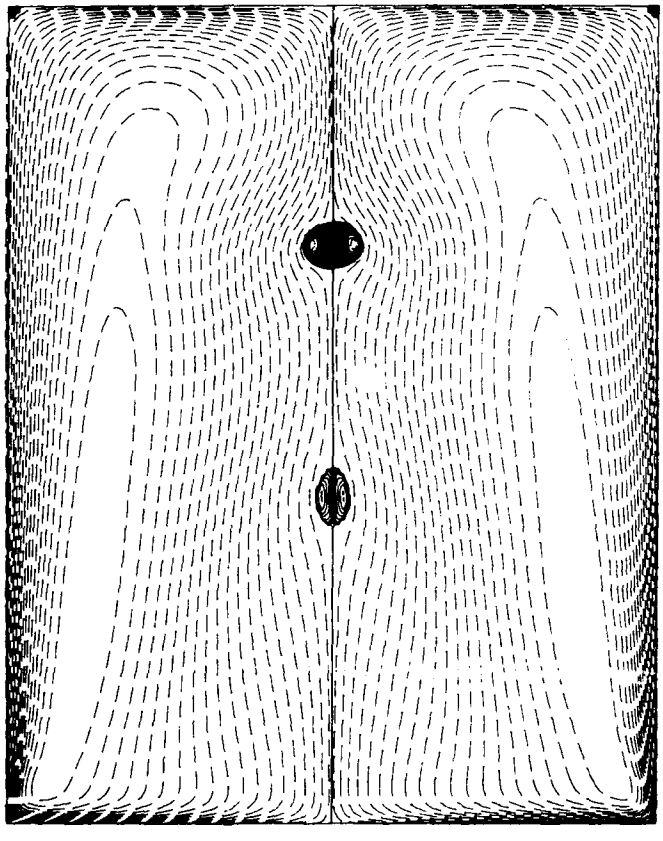

min. = -7.9×10^{-3} max. = 2.9×10^{-6}

FIGURE 2e (i)

(ii) Γ: Re = 1942 H/R = 2.5

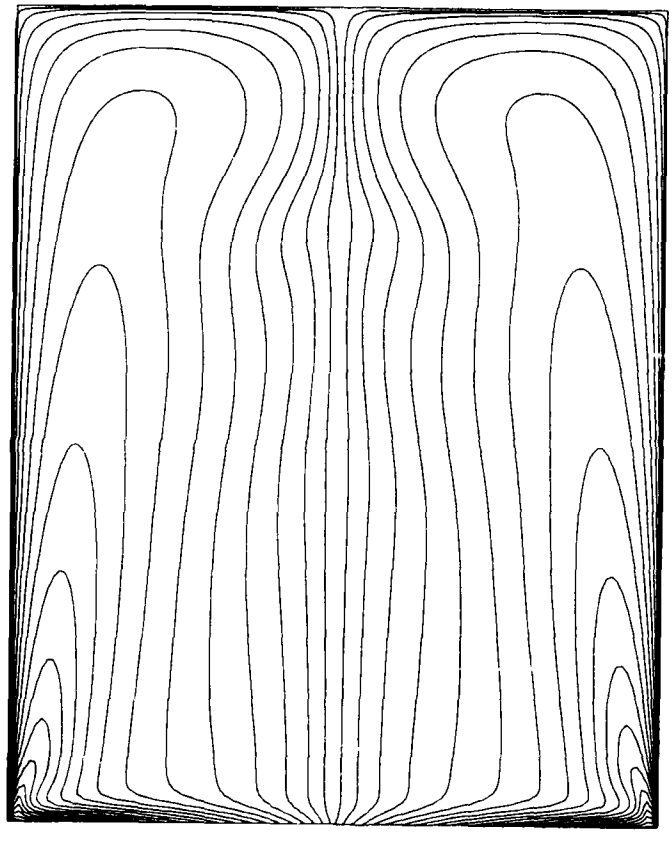

min. = 0 max. = 1.0

FIGURE 2e (ii)

(iii) η: Re = 1942 H/R = 2.5

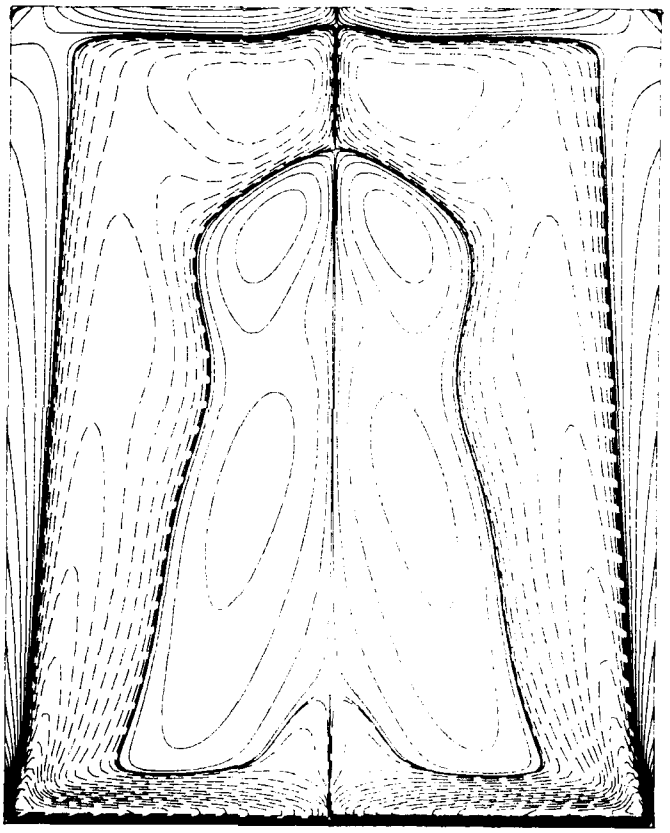

min. = -3.8 max. = 15.7

FIGURE 2e (iii)

(i) Ψ: Re = 1994 H/R = 2.5

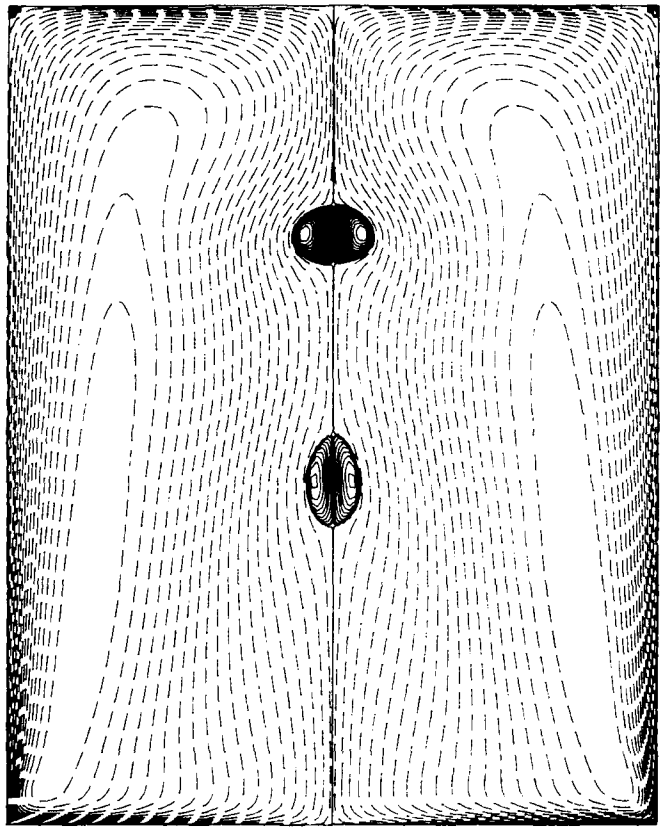

min. = -7.8×10^{-3} max. = $8.8 \times = 10^{-6}$

FIGURE 2f (i)

(ii) Γ: Re = 1994 H/R = 2.5

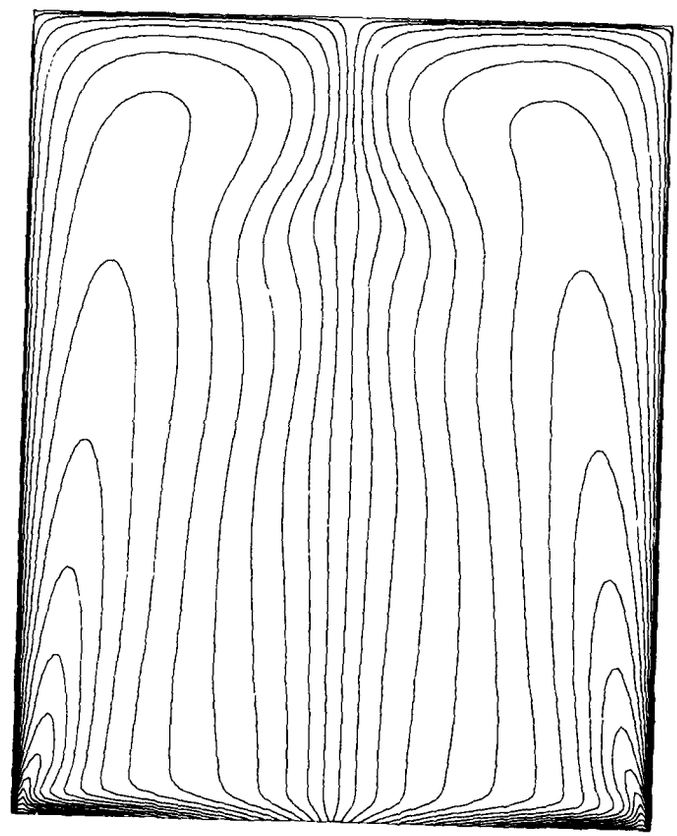

min. = 0 max. = 1.0

FIGURE 2f (ii)

(iii) η: Re = 1994 H/R = 2.5

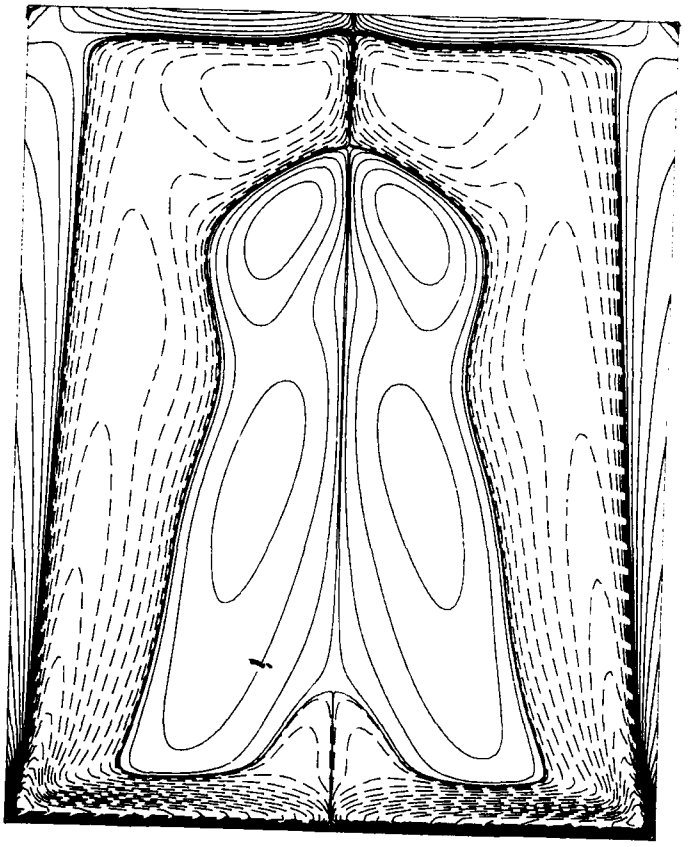

min. = -3.8 max. = 15.8

FIGURE 2f (iii)

(i) Ψ: Re=2126 H/R=2.5

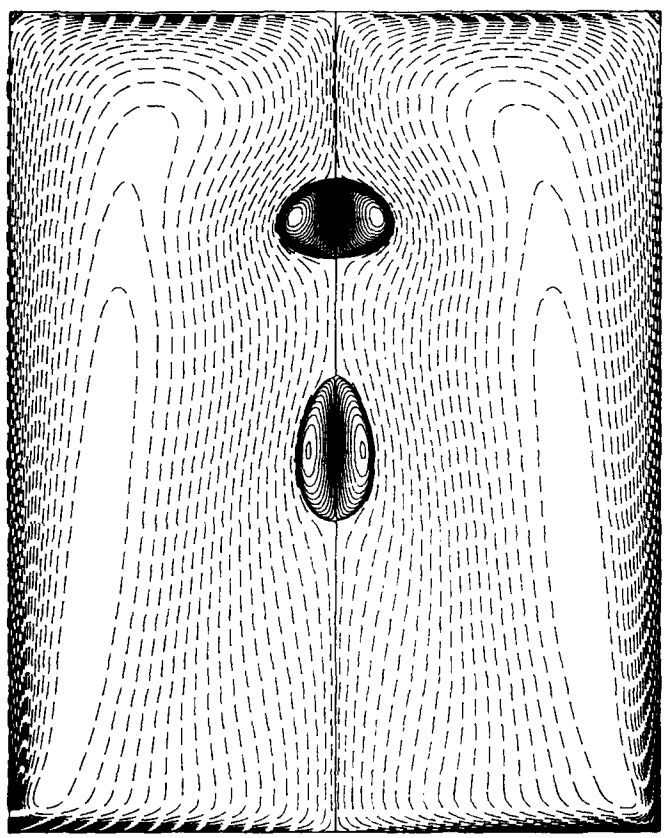

min. $=-7.6\times10^{-3}$ max. $=3.0\times10^{-5}$

FIGURE 2g (i)

(ii) Γ: Re=2126 H/R=2.5

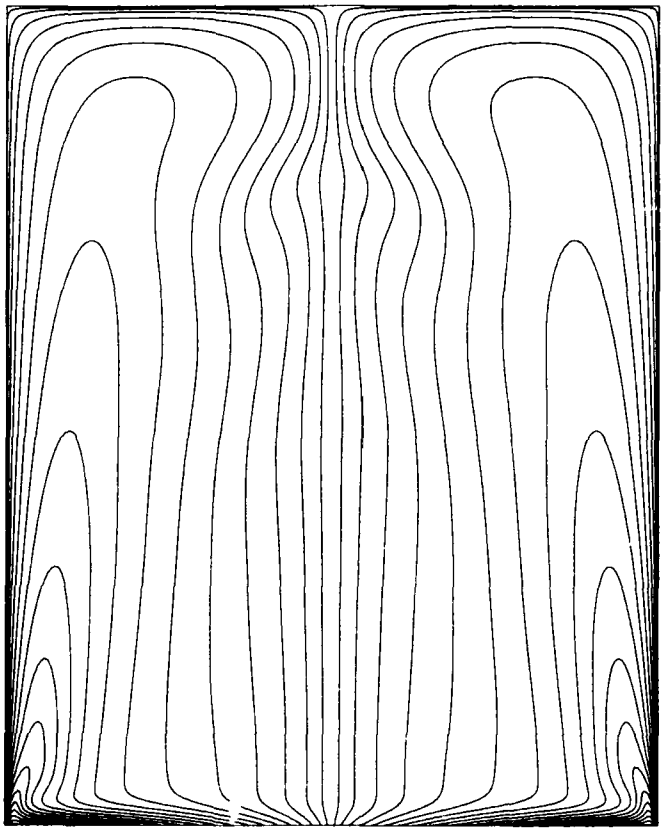

min.=0 max.=1.0

FIGURE 2g (ii)

(iii) η: Re = 2126 H/R = 2.5

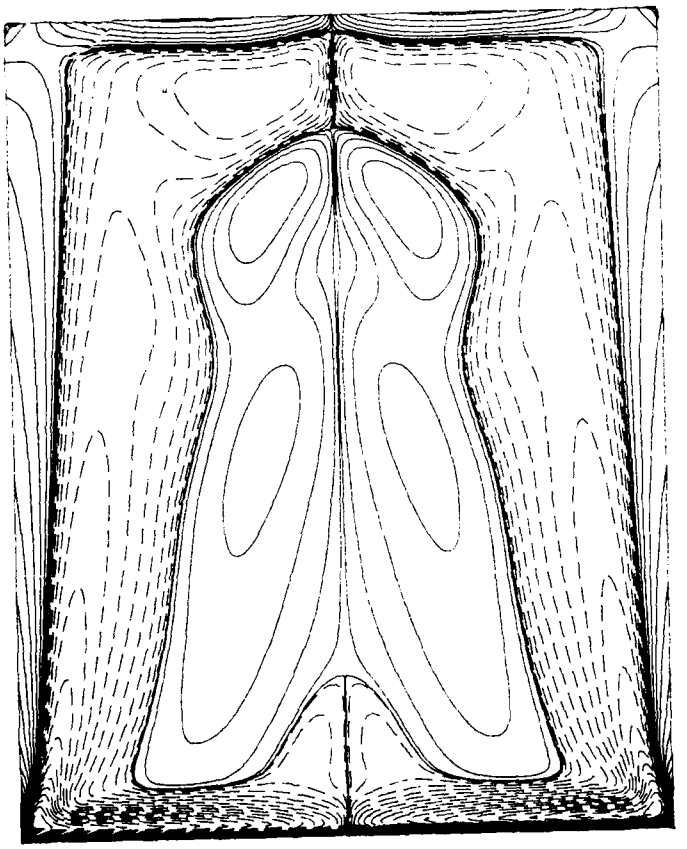

min. = -3.9 max. = 18.2

FIGURE 2g (iii)

(i) Ψ: Re=2494 R/E=2.5

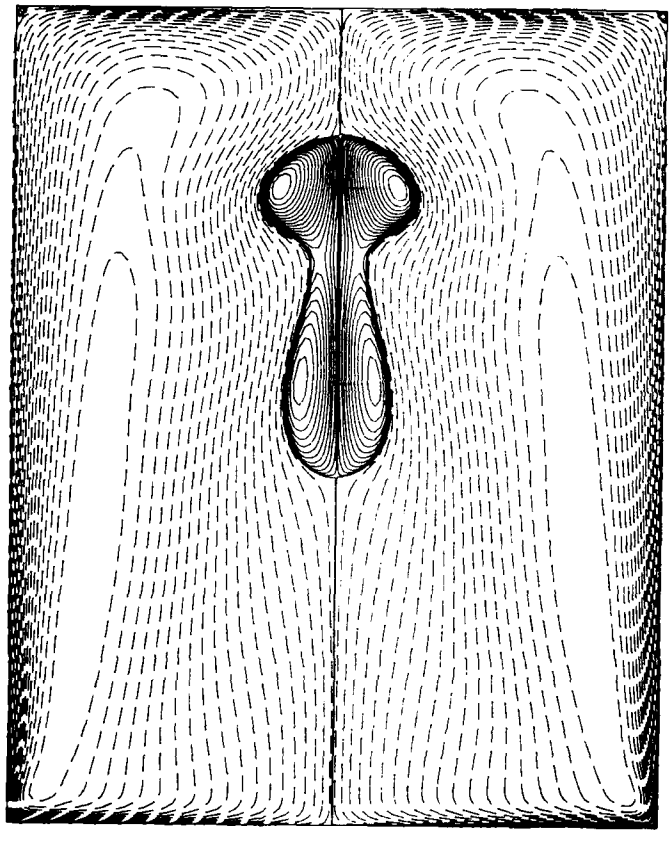

min. = -7.3×10^{-3} max. = 7.4×10^{-5}

FIGURE 2h (i)

(ii) Γ: Re=2494 H/R=2.5

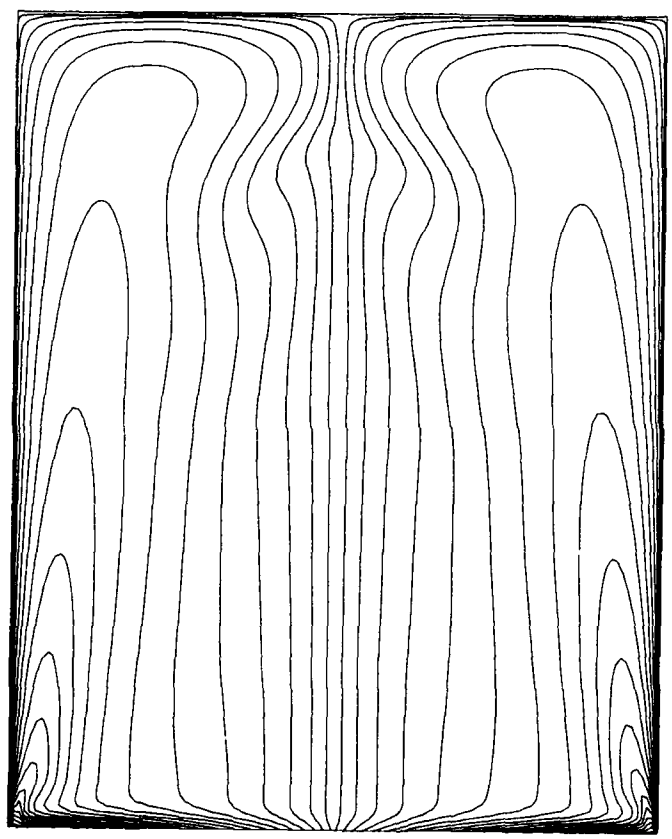

min.=0 max.=1.0

FIGURE 2h (ii)

(iii) η: Re=2494 H/R=2.5

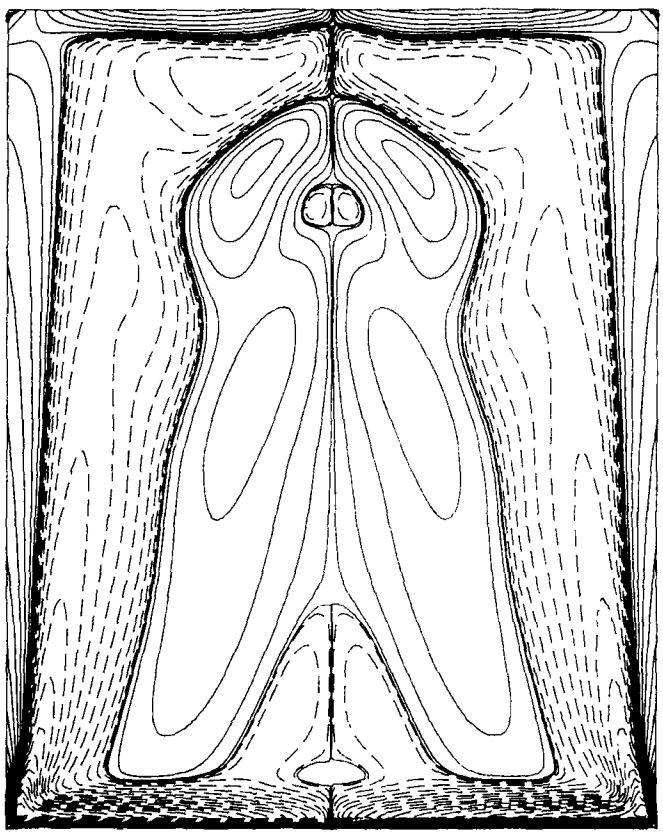

min. = -4.4 max. = 17.2

FIGURE 2h (iii)

(i) Ψ: Re=2765 H/R=2.5

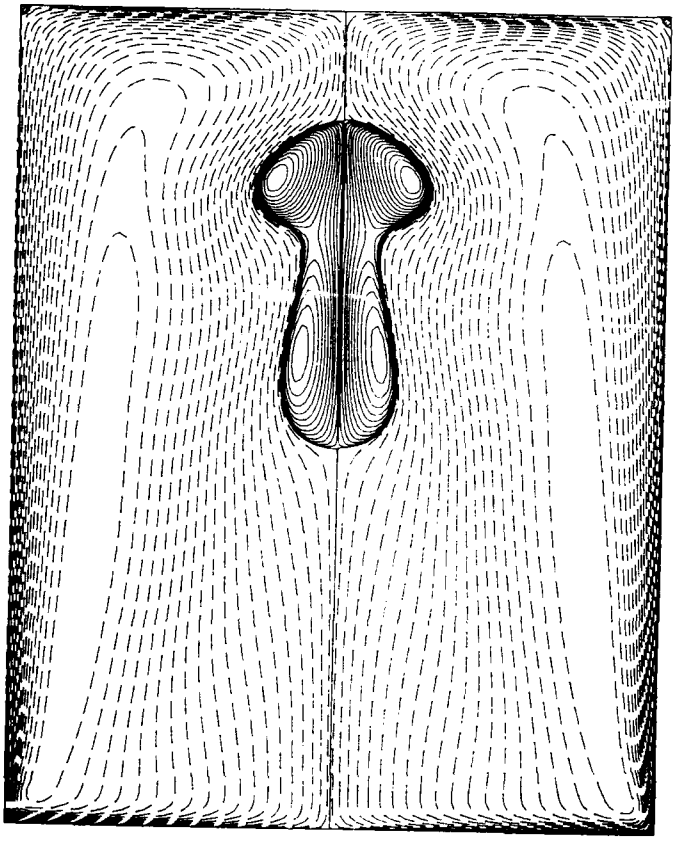

min. = -7.0×10^{-3} max. = 8.6×10^{-5}

FIGURE 2i (i)

(ii) Γ: Re=2765 H/R=2.5

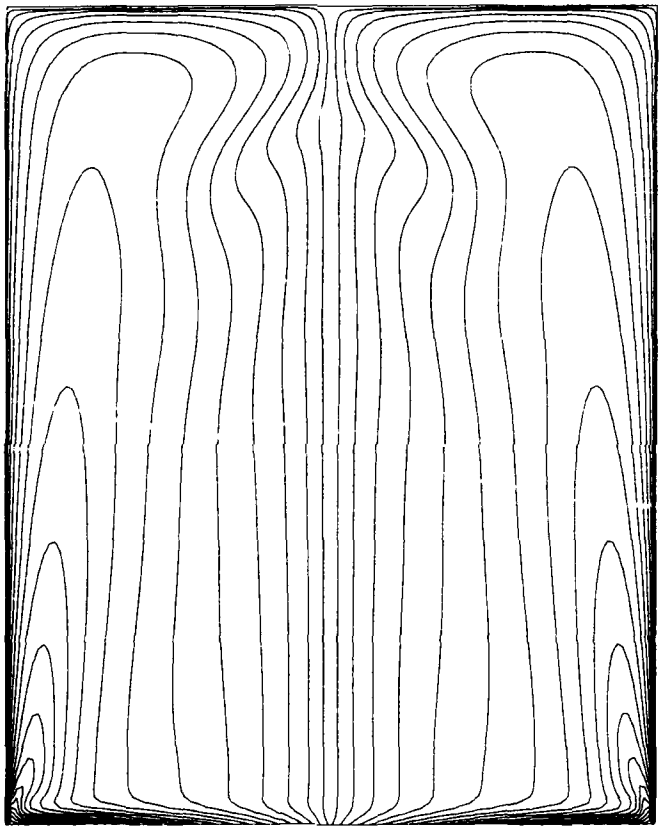

min. = 0 max. = 1.0

FIGURE 2i (ii)

(iii) η: Re=2765 H/R=2.5

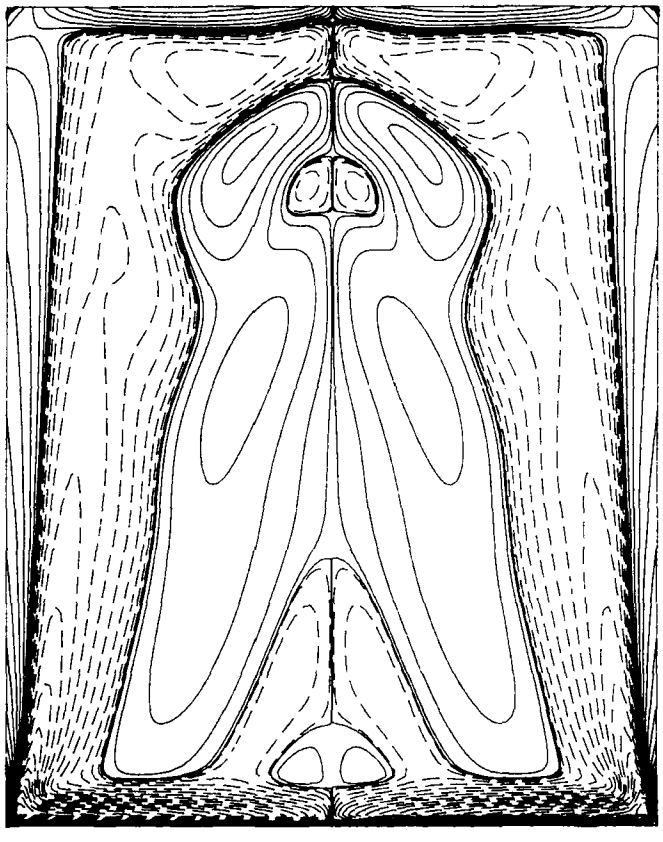

min. =-4.7 max. = 17.8

FIGURE 2*i* (iii)

FIGURE 3: VISUALIZATIONS OF THE RECIRCULATION ZONES FOR $H/R = 2.5$ AND Re AS INDICATED. * (a)AND(b) ARE REPORTED TO BE AT A STEADY STATE, WHILE (c) IS A SNAP-SHOT OF A STEADILY OSCILLATING FLOW.

3(a) $Re = 2126$
3(b) $Re = 2494$
3(c) $Re = 2765$

* ALL PHOTOGRAPHS OF THE EXPERIMENTAL VISUALIZATION ARE REPRODUCED BY KIND PERMISSION FROM M. P. ESCUDIER.

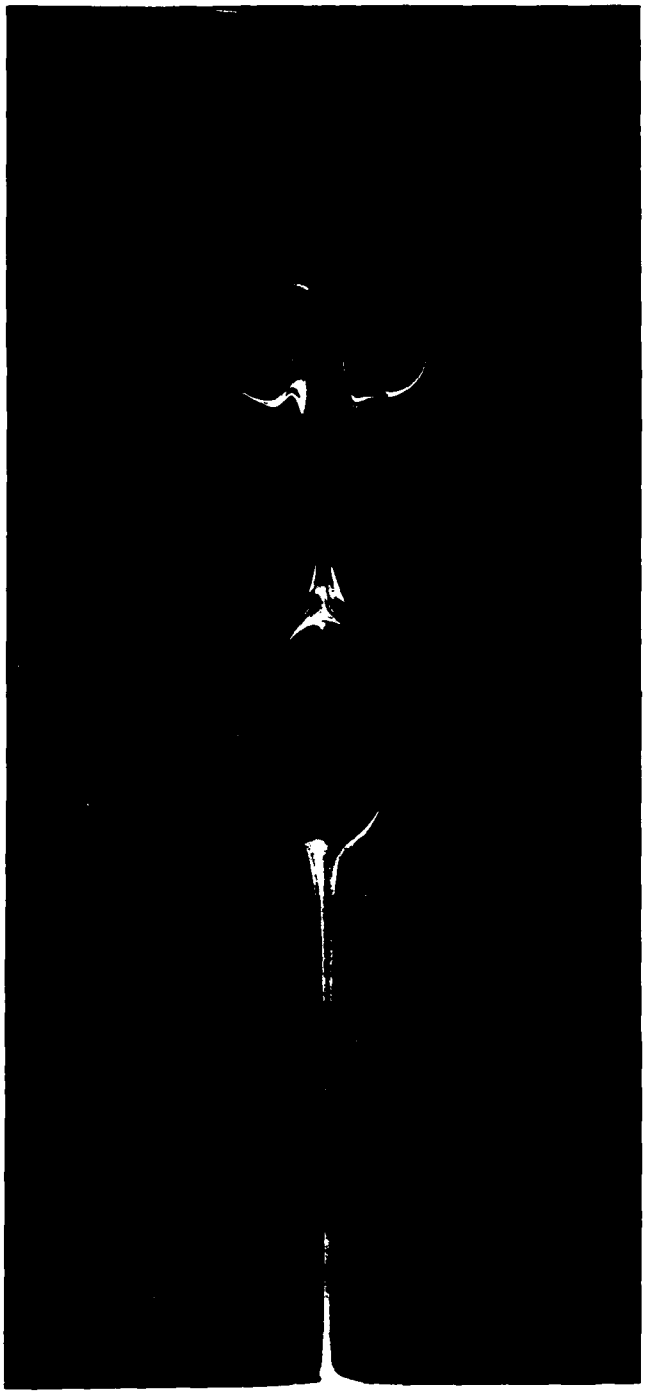

FIGURE 3a

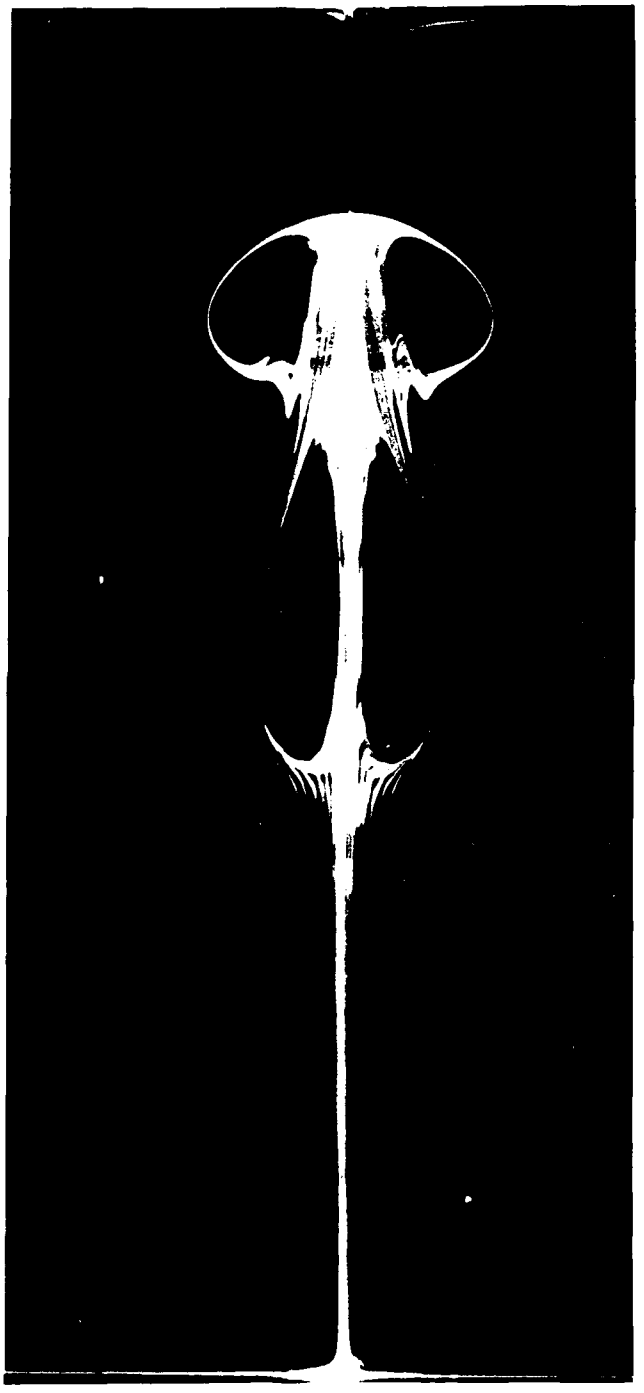

FIGURE 3b

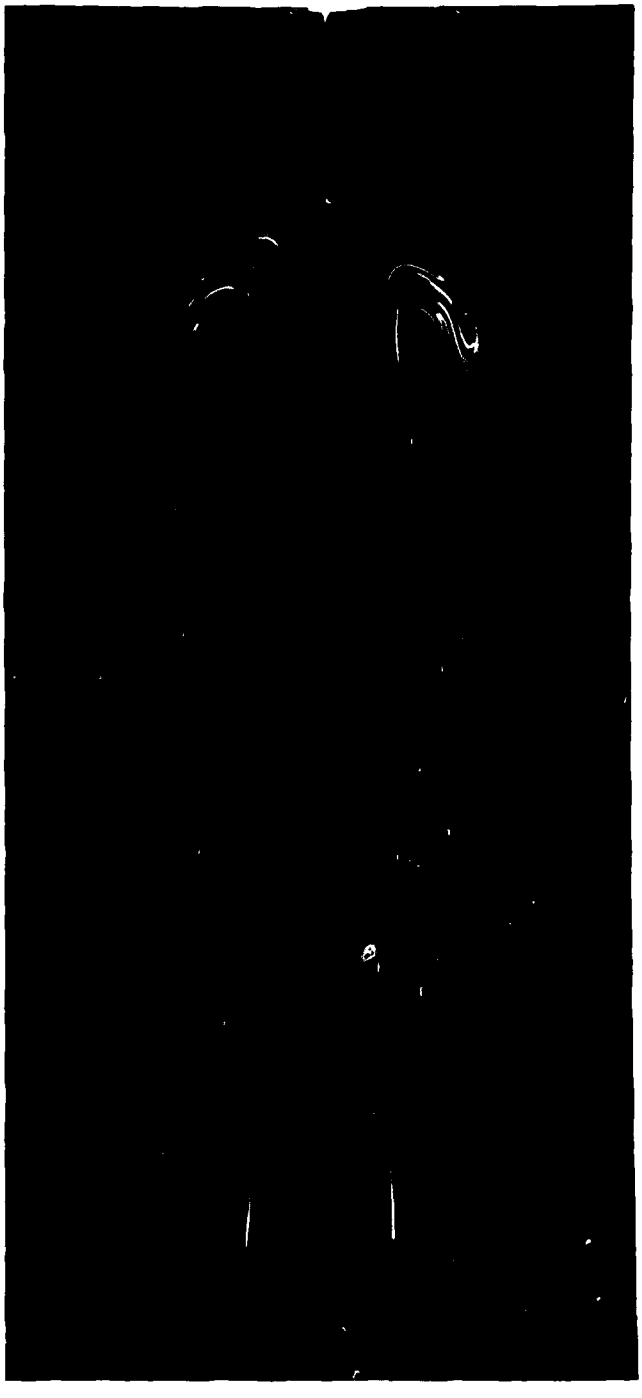

FIGURE 3c

FIGURE 4: CONTOURS OF (i) ψ, (ii) Γ AND (iii) η IN THE MERIDIONAL PLANE FOR H/R = 3.5 AND Re = 3061. THE CONTOUR LEVELS ARE NON-UNIFORMLY SPACED, WITH 20 POSITIVE AND 20 NEGATIVE LEVELS DETERMINED BY CONTOURLEVEL(i) = MAX(*variable*) × (i/20)^3 AND CONTOURLEVEL(i) = MIN(*variable*) × (i/20)^3 RESPECTIVELY. THE CONTOURS ARE OF TIME AVERAGES OVER $750 \leq t \leq 1000$.

(i) Ψ: Re=3061 H/R=3.5

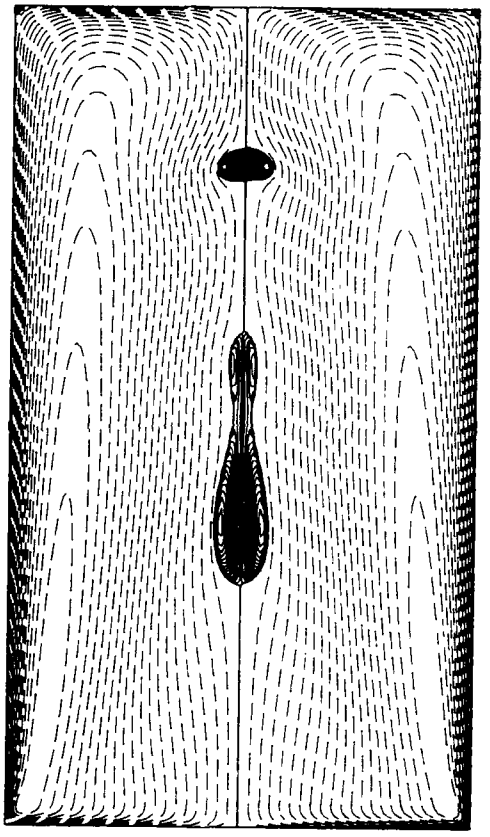

min.=-5.6×10^{-3} max.=6.3×10^{-7}

FIGURE 4 (i)

(ii) Γ: Re=3061 H/R=3.5

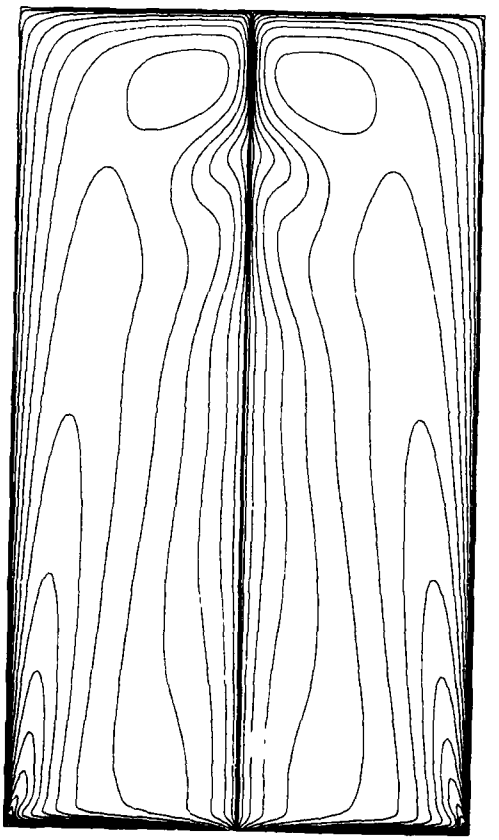

min. =0 max. = 1.0

FIGURE 4 (ii)

(iii) η: Re=3061 H/R=3.5

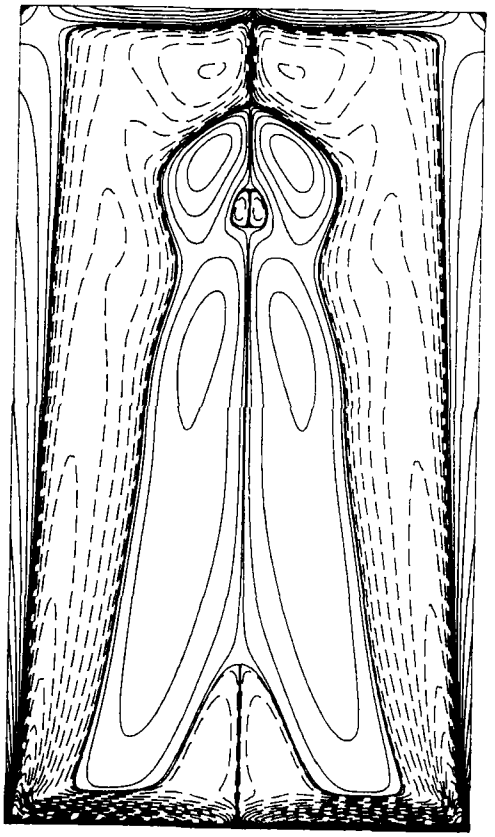

min. =-4.9 max. = 18.2

FIGURE 4 (iii)

FIGURE 5: VISUALIZATION OF THE RECIRCULATION ZONES FOR H/R = 3.5 AND Re = 3061.

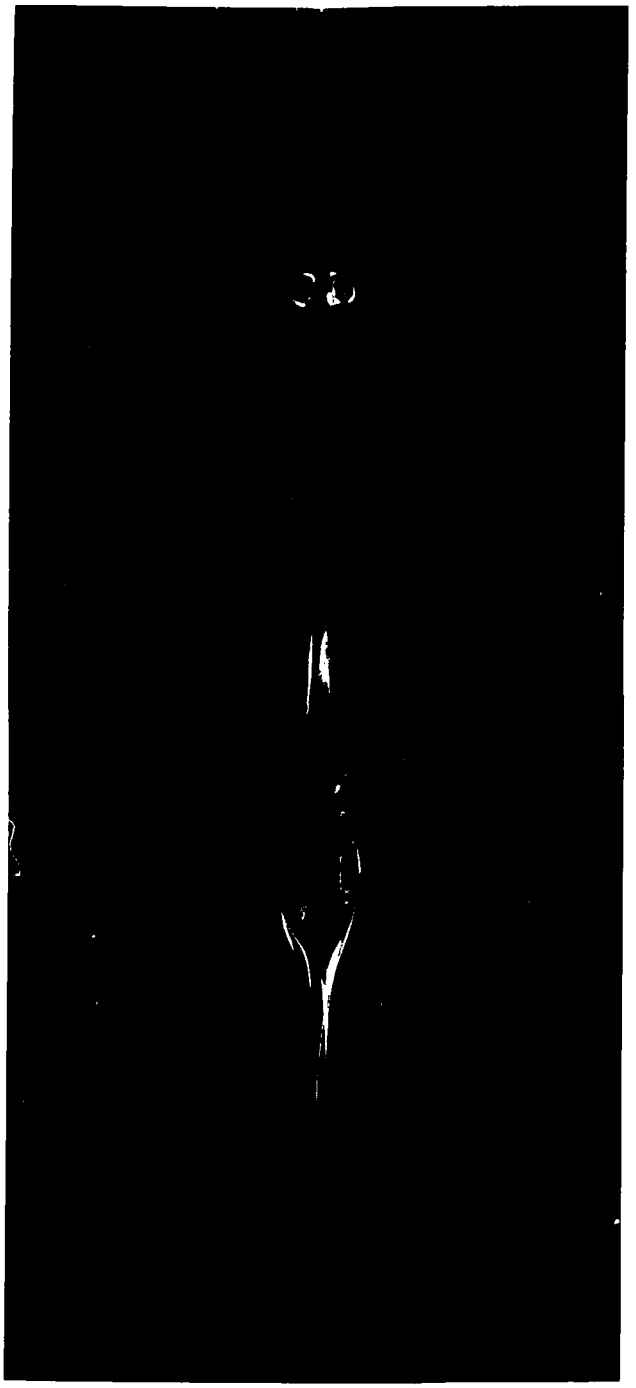

FIGURE 5

DISTRIBUTION

AUSTRALIA

Department of Defence

Defence Central
- Chief Defence Scientist
- Assist Chief Defence Scientist, Operations (shared copy)
- Assist Chief Defence Scientist, Policy (shared copy)
- Director, Departmental Publications
- Counsellor, Defence Science (London) (Doc Data Sheet Only)
- Counsellor, Defence Science (Washington) (Doc Data Sheet Only)
- S.A. to Thailand MRD (Doc Data Sheet Only)
- S.A. to DRC (Kuala Lumpur) (Doc Data Sheet Only)
- OIC TRS, Defence Central Library
- Document Exchange Centre, DISB (18 copies)

Aeronautical Research Laboratory
- Director
- Library
- Superintendent - Aerodynamics and Aero Propulsion
- Head - Aerodynamics Branch
- Divisional File - Aerodynamics and Aero Propulsion
- Author: J.M. Lopez

Defence Science & Technology Organisation - Salisbury
- Library

WSRL
- Maritime Systems Division (Sydney)

Navy Office
- Navy Scientific Adviser (3 copies Doc Data Sheet)
- Director of Naval Aircraft Engineering (Doc Data Sheet Only)

Army Office
- Scientific Adviser - Army (Doc Data sheet only)

Air Force Office
- Air Force Scientific Adviser
- Director General Aircraft Engineering - Air Force (Doc Data sheet only)

Department of Administrative Services
- Bureau of Meteorology, Library

Statutory and State Authorities and Industry
- Aerospace Technologies Australia, Manager/Librarian (2 copies)
- Hawker de Havilland Aust Pty Ltd, Bankstown, Library
- CSIRO
  - Chief, Division of Oceanography
  - Chief, Division of Energy Technology
  - Chief, Division of Atmospheric Sciences

Universities and Colleges

Adelaide
- Barr Smith Library
- Professor R.E. Luxton, Dept of Mechanical Engineering

Flinders
- Library

La Trobe
- Library

Melbourne
- Engineering Library
- Professor P.N. Joubert, Department of Mechanical Engineering
- Professor A.E. Perry, Department of Mechanical Engineering

Monash
- Hargrave Library
- Professor W.H. Melbourne, Department of Civil Engineering
- Professor B.R. Morton, Department of Mathematics

Newcastle
- Library

New England
- Library

Sydney
- Engineering Library
- Professor G.A. Bird, Department of Aeronautical Engineering

NSW
- Physical Sciences Library
- Professor R.D. Archer, Department of Aeronautical Engineering
- Professor P.T. Fink
- Library, Australian Defence Force Academy

Queensland
- Library
- Professor R.J. Stalker, Department of Mechanical Engineering

Western Australia
- Library

RMIT
- Library

CANADA

NRC

National Aeronautical Establishment
- Mr G.F. Marsters (Director)

Universities and Colleges

Toronto
- Institute for Aerospace Studies

FRANCE
ONERA, Library

GERMANY
Institute fur Stromungsmechanik der DFVLR, Professor H. Ludwieg

INDIA
National Aeronautical Laboratory,
Professor R. Nasasimha (Director)

ISRAEL
Technion-Israel Institute of Technology
Professor J. Singer

JAPAN
National Aerospace Laboratory

NETHERLANDS
National Aerospace Laboratory (NLR), Library

SWEDEN
Aeronautical Research Institute, Library

SWITZERLAND
Brown, Boveri, and Co., Dr J.J. Keller

UNITED KINGDOM
Royal Aircraft Establishment, Farnborough
Director, Dr G.G. Pope,
Dr M.G. Hall
British Aerospace
Kingston-upon-Thames, Library
Schlumberger Cambridge Research Ltd., Dr M.P. Escudier

Universities and Colleges
Cambridge
Library, Engineering Department
Professor G.K. Batchelor

Oxford
Professor T.B. Benjamin

Cranfield Inst. of Technology
Library
Professor J.L. Stollery

Imperial College
Aeronautics Library
Professor P. Bradshaw
Professor J.T. Stuart

UNITED STATES OF AMERICA
NASA Scientific and Technical Information Facility
Director NASA Langley, Mr R.H. Peterson

Director NASA Lewis, Dr T.M. Klineberg
Director NASA Ames, Dr W.F. Ballhaus, Jr.
Boeing Company, Library
United Technologies Corporation, Library
Lockheed-California Company
Lockheed Missiles and Space Company
Lockheed Georgia
McDonnell Aircraft Company, Library
McDonald Douglas Research Laboratory, Director

Universities and Colleges

Massachusetts Inst. of Technology
Professor M.T. Landahl

CALTECH
Professor P.G. Saffman
Professor H.G. Hornung
Professor A. Roshko

Cornell
Professor S. Leibovich

Stanford
Professor W.C. Reynolds
Professor S.J. Kline
Professor B.J. Cantwell

Naval Post-Graduate School
Profesor T. Sarpkaya

Spares (20 copies)
TOTAL (122 copies)

AL 149
REVISED DECEMBER 87

DEPARTMENT OF DEFENCE

DOCUMENT CONTROL DATA

PAGE CLASSIFICATION: UNCLASSIFIED

PRIVACY MARKING:

1a. AR NUMBER	1b. ESTABLISHMENT NUMBER	2. DOCUMENT DATE	3. TASK NUMBER
AR-004-572	ARL-AERO-R-173	JANUARY 1988	DST 85/025

4. TITLE

AXISYMMETRIC VORTEX BREAKDOWN PART I: CONFINED SWIRLING FLOW

5. SECURITY CLASSIFICATION

(PLACE APPROPRIATE CLASSIFICATION IN BOX(S) IE. SECRET (S), CONFIDENTIAL (C), RESTRICTED (R), UNCLASSIFIED (U) .)

DOCUMENT	TITLE	ABSTRACT
U	U	U

6. No. PAGES: 61

7. No. REFS.: 19

8. AUTHOR(S)

J.M. LOPEZ

9. DOWNGRADING/DELIMITING INSTRUCTIONS

10. CORPORATE AUTHOR AND ADDRESS

AERONAUTICAL RESEARCH LABORATORY
P.O. BOX 433, MELBOURNE VIC. 3001

11. OFFICE/POSITION RESPONSIBLE FOR

SPONSOR: DSTO
SECURITY:
DOWNGRADING:
APPROVAL:

12. SECONDARY DISTRIBUTION (OF THIS DOCUMENT)

Approved for public release.

OVERSEAS ENQUIRIES OUTSIDE STATED LIMITATIONS SHOULD BE REFERRED THROUGH ASDIS, DEFENCE INFORMATION SERVICES BRANCH, DEPARTMENT OF DEFENCE, CAMPBELL PARK, CANBERRA, ACT 2601

13a. THIS DOCUMENT MAY BE ANNOUNCED IN CATALOGUES AND AWARENESS SERVICES AVAILABLE TO.....

No limitations

13b. CITATION FOR OTHER PURPOSES (IE. CASUAL ANNOUNCEMENT) MAY BE [X] **UNRESTRICTED OR** [ ] **AS FOR 13a.**

14. DESCRIPTORS

Vortex breakdown
Flow visualization
Navier-Stokes equations

15. DRDA SUBJECT CATEGORIES

0046B
0051A

16. ABSTRACT

A comparison between the experimental visualization and numerical simulations of the occurrence of vortex breakdown in laminar swirling flows produced by a rotating endwall is presented. The experimental visualizations of Escudier (Experiments in Fluids, 2, 1984) were the first to detect the presence of multiple recirculation zones and the numerical model presented here, consisting of a numerical solution of the unsteady axisymmetric Navier-Stokes equations, faithfully reproduces these newly observed phenomena and all other observed characteristics of the flow. Part II of the paper examines the underlying physics of these vortex flows.

PAGE CLASSIFICATION
UNCLASSIFIED
PRIVACY MARKING

THIS PAGE IS TO BE USED TO RECORD INFORMATION WHICH IS REQUIRED BY THE ESTABLISHMENT FOR ITS OWN USE BUT WHICH WILL NOT BE ADDED TO THE DISTIS DATA UNLESS SPECIFICALLY REQUESTED.

16. ABSTRACT (CONT.)

17. IMPRINT

AERONAUTICAL RESEARCH LABORATORY, MELBOURNE

18. DOCUMENT SERIES AND NUMBER	19. COST CODE	20. TYPE OF REPORT AND PERIOD COVERED
AERODYNAMICS REPORT 173	54 5006	

21. COMPUTER PROGRAMS USED

22. ESTABLISHMENT FILE REF. (S)

23. ADDITIONAL INFORMATION (AS REQUIRED)